

## INFRARED AND OPTICAL MORPHOLOGIES OF DISTANT RADIO GALAXIES

M. A. RIGLER<sup>1,2,3</sup>

Institute for Astronomy, University of Hawaii

S. J. LILLY<sup>1,2,3</sup>

Institute of Astronomy, University of Hawaii and Department of Astronomy, University of Toronto

A. STOCKTON<sup>1</sup>

Institute for Astronomy, University of Hawaii

F. HAMMER<sup>1</sup>

DAEC, Observatoire de Paris-Meudon

AND

O. LE FÈVRE

Canada-France-Hawaii Telescope Corporation and Observatoire de Paris-Meudon

Received 1991 February 25; accepted 1991 August 1

### ABSTRACT

Multicolor line and continuum images of a complete sample of 13 3C radio galaxies at  $0.8 < z < 1.3$ , spanning the range  $2500 \text{ \AA}$  to  $1 \text{ }\mu\text{m}$  in the rest frame, are presented and analyzed. Quantitative analysis of these images shows that the infrared images are less elongated than those at optical wavelengths and show only a much weaker “alignment effect” with the radio source axis. The quadrupole moments show a progressive reduction from short to long wavelengths, as expected if a symmetric component dominates at infrared wavelengths. A spectral decomposition based on these moments suggests that the aligned component probably has a roughly flat spectral energy distribution in  $f_\nu$ , while the symmetric red component that dominates in the infrared probably has a spectral energy distribution similar to that of a gE galaxy. In typical 3C galaxies at  $z = 1$ , the active aligned component contributes 10% of the infrared light. While more active objects have a larger contamination, these generally modest components are insufficient to perturb significantly either the scatter in, or the continuity of, the observed  $K$ - $z$  relation. The conventional interpretation of the  $K$ - $z$  diagram in terms of a uniform population of mature host galaxies is thus still likely to be correct. As far as can be determined from the data, the scale sizes of the radio galaxy images at infrared wavelengths are consistent with the sizes of the giant ellipticals associated with powerful radio galaxies at low redshift. Several of these radio galaxies are accompanied by small red companion galaxies that are prominent on our infrared images at random position angles relative to the radio axis. These are interpreted as representing a conventional trigger for the radio sources. There is a preference for these companions to be associated with the bluest, most aligned, and generally most active objects.

*Subject headings:* galaxies: evolution — galaxies: photometry — galaxies: stellar content — radio continuum: galaxies

### 1. INTRODUCTION

The increasing number of radio galaxies that have been found at  $z \gg 1$ , including several examples with  $z > 3$  (Lilly 1988; Rawlings, Eales, & Warren 1990; Chambers, Miley, & van Breugel 1990; McCarthy et al. 1991; H. Spinrad 1990, private communication) has led to increased interest in the evolutionary status of these remote galaxies. At present, radio galaxies offer an unparalleled opportunity to study stellar populations at early epochs in the universe.

The basic optical-infrared photometric properties of powerful radio galaxies at  $z > 1$  were established some time ago (Lilly & Longair 1984; Eisenhardt & Lebofsky 1987; Dunlop

et al. 1989; Lilly 1989). In the near-infrared  $K$ -band, which samples a rest wavelength of around  $1 \text{ }\mu\text{m}$  at  $z = 1$ , the radio galaxies appear to be remarkably homogeneous. Single-element photometry with large  $8''$ – $12''$  apertures of complete 3C and “1 jansky” samples (Lilly & Longair 1984; Lilly, Longair, & Allington-Smith 1985; Lilly 1989) shows, from very low redshifts to at least  $z = 2$ : (a) a small dispersion in the  $K$ -band absolute magnitude of only 0.4–0.5 mag (at a given redshift) and (b) a striking continuity in mean absolute magnitude with redshift. In contrast, a wide range of optical-infrared colors is observed, indicating a large variation in ultraviolet luminosities at  $\lambda < 3000 \text{ \AA}$ . Some radio galaxies at  $z > 1$ , such as 3C 65, have optical-infrared colors that are not much bluer than those of unevolving elliptical galaxies, while others, like 3C 368, have the colors of Irr galaxies. This uniformity in the rest-frame red/visual and the wide variation in the rest-frame ultraviolet have generally been interpreted (Lilly & Longair 1984; Lilly 1989) in terms of a homogeneous population of host galaxies, selected by a mass-selection function that works in a similar fashion over the whole interval  $0 < z < 3$  and selects from a population of massive galaxies of roughly

<sup>1</sup> Visiting Astronomer at the Canada-France-Hawaii Telescope, which is operated by the National Research Council of Canada, the Centre National de Recherche Scientifique of France, and the University of Hawaii.

<sup>2</sup> Visiting Astronomer, United Kingdom Infrared Telescope, which is operated by the Royal Observatory Edinburgh on behalf of the United Kingdom Science and Engineering Research Council.

<sup>3</sup> Visiting Astronomer, Infrared Telescope Facility, which is operated by the University of Hawaii on behalf of the National Aeronautics and Space Administration.

uniform age at a given epoch, so that the mass-to-light ratio smoothly varies with redshift. In this picture, a blue galaxy such as 3C 368 is interpreted as being as old as the much redder 3C 65, but with a much stronger rejuvenating burst of star formation rather than as an intrinsically young system. In this interpretation, the light from this older population dominates the long-wavelength continuum emission and is responsible for the small scatter in the  $K$ -band. The ultraviolet light, which shows the large variations from galaxy to galaxy, has generally been ascribed to a very young stellar population produced in a vigorous burst of star formation, possibly associated with the radio activity, though other forms of ultraviolet activity cannot be ruled out at this time.

We will henceforth refer to this interpretation as the “old galaxy hypothesis.” The key element of this idea is that the small dispersion in the  $K$ - $z$  relation arises because of the dominance in the infrared wave band of a homogeneous population of host galaxies. Consequently, in this view, the age of all the radio galaxies at a given redshift is constrained by the colors of the reddest object in the sample: At  $z = 1$ , this is 3C 65, which has an implied minimum age of  $2 \times 10^9$  yr (Chambers & Charlot 1990), suggesting  $z_F > 2.2$  (for  $\Omega_0 = 1$  and  $H_0 = 50 \text{ km s}^{-1} \text{ Mpc}^{-1}$ ). If the continuity of the  $K$ - $z$  relation is taken seriously as indicating a steady evolution in luminosity, then we can infer that the radio galaxies at  $z = 1$  formed at even higher redshifts, i.e.,  $z_F > 5$  as inferred from the  $3\text{--}4 \times 10^9$  yr ages of the radio galaxies at  $z \sim 3.5$  (Lilly 1988; Chambers & Charlot 1990). It should be noted that the old galaxy hypothesis makes no statement *per se* about the nature of the ultraviolet continuum. If it is correct, the old galaxy hypothesis has important ramifications for our understanding of galaxy formation, for two reasons. First, it provides one of the strongest indications that the universe at  $z > 1$  is basically similar to the local universe—at least one class of galaxies has very similar properties at very high redshifts (at least at long wavelengths) compared with nearby galaxies selected in similar way. Second, if it can be extended to the newly found systems at  $z > 3$ , then it demonstrates that at least some massive galaxies formed at very early times in the universe.

Recently, detailed observations of the morphologies and spectra of the ever-increasing number of radio galaxies identified at  $z \gg 1$  have led to both refinements of, and challenges to, this basic picture. First, McCarthy et al. (1987b) and Chambers, Miley, & van Breugel (1987) discovered that the optical continuum (i.e., the rest-frame ultraviolet) and the  $[\text{O II}] \lambda 3727$  emission of a large fraction of radio galaxies at  $z > 0.8$  are aligned with the axis of the radio source in a way not encountered at low redshift. These authors interpreted this “alignment effect” as due to star formation induced by the passage of the radio jet, and several theoretical explorations of this effect have been made (de Young 1989; Rees 1989; Daly 1990a).

Chambers & McCarthy (1990) have presented evidence that young stars are indeed responsible for the ultraviolet emission by co-adding the spectra of different radio galaxies, and have claimed to discern in the integrated spectrum “stellar” absorption lines. On the other hand, di Serego Alighieri et al. (1989) and Scarrott, Rolph, & Tadhunter (1990) have detected significant polarization in 3C 168 and 3C 277.3. This observation supports the idea that the aligned continuum emission is scattered light from an anisotropically emitting nucleus, as might be produced in the hypothesis recently revived by Barthel (1989) that unifies radio galaxies and quasars through orienta-

tion effects. In the case of the line emission, van Breugel & McCarthy (1990) have also argued that the line ratios favor a relatively hard ionizing spectrum and that the required ionizing flux necessitates an obscured nucleus, given the absence of a bright nuclear source of ultraviolet emission. Thus there is continuing debate on the origin of the ultraviolet continuum, the cause of the ultraviolet alignment effect, and the relative importance of stellar and nonstellar emission at short wavelengths. Of course, several different phenomena may well be occurring in practice.

In parallel with these studies, there has also been considerable attention paid to the so-called Lyman- $\alpha$  galaxies, and in particular to objects such as 3C 326.1 at  $z = 1.8$ , which was claimed by McCarthy et al. (1987b) to represent a new class of gaseous radio galaxy in which the bulk of the stellar population had yet to form. However, infrared observations of this object (Lilly & McLean 1989) reveal a compact component coincident with one of McCarthy et al.’s “knots.” This object is located between the radio lobes and has similar photometric properties to other radio galaxies. This suggests that it contains a substantial stellar population of moderate age and hence that it should not be considered a forming protogalaxy. This object therefore now fits in with the old galaxy hypothesis, at least with respect to its broad photometric properties.

Nevertheless, the association of the red/visual (i.e., observed  $K$ -band) light in the high-redshift radio galaxies with the photospheric emission of stars in mature and homogeneous stellar populations (central to the old galaxy hypothesis) has been challenged because of perceived difficulties in accounting for the infrared morphologies. The recent implementation of sensitive two-dimensional array detectors operating in the near-infrared wave band has allowed the study of the morphology of these systems. In several cases, these appear to show alignment effects with the radio source axes (see below). Alternative models have been advanced, and two, which involve young stellar populations, merit particular attention.

In the first model, Chambers & Charlot (1990) have argued that the bluer radio galaxies may in fact be much younger systems than the redder ones. We will refer to this as the “range of ages model.” They showed that, for a particular choice of the initial mass function, the evolution in the red/visual luminosity with age may be made small enough that the small dispersion in  $K$  may be preserved even with a large range in age within the radio galaxy sample (e.g.,  $3 \times 10^8$  yr for 3C 368 to  $2 \times 10^9$  yr for 3C 65, both at  $z = 1.1$  and both with  $K = 17$ ). Of course, a tight mass-selection effect must still operate, and this may be difficult to explain over the wide range of dynamical ages represented by the systems in this picture (from  $\sim 1$  dynamical time scale for 3C 368 to  $\sim 100$  times longer for radio galaxies at low redshifts). This range-of-ages interpretation has always been a possibility (the stellar population models have not changed substantially over the last few years) but was originally rejected by Lilly & Longair (1984) because it was believed that it would lead to an unacceptably high dispersion in the  $K$ - $z$  relation. Indeed, Lilly (1989), making the assumption that the run of absolute magnitude with redshift in the  $K$ - $z$  diagram was entirely due to an evolving mass-to-light ratio, argued that the spread in age within the radio galaxy population at  $z = 1.5$  could be no more than  $\Delta\tau/\tau \approx 25\%$  and was in all likelihood somewhat less. Chambers & Charlot’s (1990) conclusion is dependent on the choice of the initial mass function and, to a lesser extent, the star formation history, although the requirements are not

unreasonable. In passing, it should be noted that the reduction in the minimum age of the  $z = 3.4$  radio galaxy 0902+34 to  $4 \times 10^8$  yr (Chambers & Charlot 1990) from the 1 Gyr age proposed earlier (see Lilly 1988) was primarily due to a reduction in the  $K$  brightness by about 1 mag (Lilly 1990) rather than to any particular feature of the evolutionary models used.

Noting that the blue radio galaxies such as 3C 368 may, on the basis of their broad-band colors, be only  $3 \times 10^8$  yr old, Chambers & Charlot (1990) have suggested that the interaction of radio jets with the ambient gaseous medium may be a dominant process in the formation of massive galaxies. On the other hand, Daly (1992) and Leahy (1990) have both pointed out time-scale difficulties with this scheme based on the radio source lifetimes, which they estimated to be of order a few times  $10^7$  years for typical 3C sources at  $z = 1$  (see also Alexander & Leahy 1987). Hence, even in the case of 3C 368, which is inferred to have a minimum age of  $3 \times 10^8$  yr (Chambers & Charlot 1990), the bulk of the galaxy must have been formed in previous, more vigorous, episodes of the radio source, and this removes some of the appeal of this model.

In the second model, Bithell & Rees (1990) have advocated a quite different scheme in which the  $K$ -band light comes from extremely young populations ( $10^7$  yr) of red supergiants. The ages of these populations are then fully consistent with the lifetime of a single outburst of the radio source. These authors suggested that the observed range of colors could represent different phases of a rapidly evolving stellar population of extreme youth. Given that an individual massive star produces most of its bolometric luminosity as a blue supergiant (Chiosi & Maeder 1986), the circumstances for domination by red supergiants to occur are very contrived—requiring a very narrow range of stellar masses and ages (see Lilly 1990). The rapid evolution of this population would certainly produce a wide range in mass-to-light ratios and hence an unacceptably large scatter in the  $K$ - $z$  diagram.

In attempting to distinguish experimentally between the old galaxy model and the range-of-ages model, it should be realized that, as defined above, they represent extreme positions. Indeed the definition of the age of a stellar population is clearly somewhat ambiguous in the face of what may be quite large bursts of star formation. Few would deny that 3C 368 is younger than 3C 65 if a *luminosity*-weighted average of the stellar population is taken, but a *mass*-weighted average would produce comparable ages if the old galaxy model is correct. While the true situation may be somewhat blurred between these extremes, the conceptual distinction is clear, and the question of whether the bluest galaxies contain an old stellar population similar to that in the reddest galaxies is clearly of great importance to our view of the formation of massive galaxies.

Much of the motivation for the theoretical work described above has come from infrared imaging observations. The morphology at infrared wavelengths clearly offers a decisive test of the old galaxy hypothesis. The mature galaxy component that is assumed to underlie the aligned active component should be dynamically relaxed and should not display significant morphological peculiarities. If peculiarities are seen, then this is a strong argument for either much younger stellar ages, i.e., shorter than the dynamical time scale for the system, or for a nonstellar origin for the infrared light. We stress that the old galaxy hypothesis is *not necessarily* invalidated by the presence of an aligned component in infrared images, regardless of its

color. The test, rather, is to *determine whether these morphologically peculiar components produce so much of the large-aperture integrated light that the conventional interpretation of the small scatter in the infrared Hubble diagram in terms of mature underlying host galaxies can be ruled out.*

Several studies of the infrared morphologies of limited samples of objects—3C 368 (Chambers, Miley, & Joyce 1988a; Djorgovski et al. 1991), 3C 356 (Eales & Rawlings 1990), and a sample of eight 3C radio galaxies with  $0.7 < z < 1.8$  (Eisenhardt & Chokshi 1990) have been carried out. These authors have all found some “infrared alignment” in the radio galaxies and have concluded with varying degrees of conviction that the infrared light could not be dominated by old stars to the degree required to produce the small scatter in the  $K$ - $z$  relation. Two criticisms may, however, be applied to these early papers. First, there has been very little attempt at quantitative analysis. Clearly, unless the aligned component is implausibly blue, it must contribute some significant fraction of the  $K$ -band light. If the aligned component has high surface brightness relative to the more diffuse outer regions of an extended underlying galaxy, it may produce dramatic morphological peculiarities and yet contribute a relatively small fraction of the total light. As an example, Lilly (1989) decomposed the overall spectral energy distributions of high- $z$  radio galaxies into the sum of an Irr plus a gE galaxy. In this heuristic exercise, the fraction of the  $K$ -band light that came from the blue, potentially aligned, Irr component was designated  $f_K$ . In the 3C sample at high redshifts, the average value of  $f_K$  was 20%, with a dispersion within the sample of 10% and a maximum of about 40% in the case of very blue objects like 3C 368. Clearly, a  $20\% \pm 10\%$  contribution from an active component would not significantly perturb the scatter in the  $K$ - $z$  relation which will have an intrinsic dispersion of order 0.4 mag. Of course, the aligned component could in reality have a different spectral energy distribution than that of an Irr galaxy, which would lead to different levels of contamination.

The potentially large morphological effects of components with relatively minor contributions to the total light are illustrated in Figure 1 (*upper panel*). We have constructed model radio galaxies in which we have combined a round component with a de Vaucouleurs profile ( $r_w = 2''$ ) and an aligned component, assumed to be one-dimensional and of length  $4''$ . These have been smoothed with a Gaussian point-spread function of  $1''$  FWHM. Models in which 0%, 20%, and 50% of the light within a  $4''$  aperture is contributed by the aligned component are shown in Figure 1. It can be seen that a 20% linear contribution can produce a strikingly aligned image, yet will not perturb the scatter in the  $K$ - $z$  relation. An aligned component that was more concentrated toward the outer regions would have a correspondingly larger morphological effect. We return to these models later when a quantitative measure of asymmetry is developed.

The likely contamination from the aligned component makes a quantitative analysis absolutely essential in order to see whether the morphological peculiarities are due to this contamination alone.

The second criticism is that only a few generally nonrepresentative objects have been observed, although the conclusions drawn from them have frequently been applied to the population as a whole. For instance, 3C 368 has often been taken as a prototype for high-redshift radio galaxies. In fact, as noted above, it is a very *extreme* object. It has the bluest ( $r - K$ ) color, and among the strongest emission lines, in the Lilly & Longair

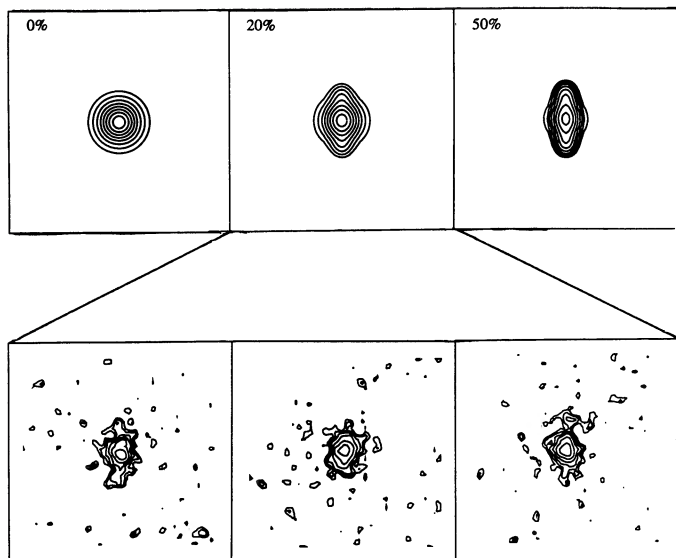


FIG. 1.—Effects of adding a linear component to a symmetric host galaxy with a de Vaucouleurs profile. Each image is  $15''$  square and has been smoothed with a Gaussian of  $1''$  FWHM. The upper panels show composite galaxies in which the linear component contributes 0%, 20%, and 50% of the total flux in a  $4''$  aperture. The lower panels show the effect of adding noise to the 20% simulation. The noise has similar characteristics to that in our real data.

(1984) sample. In addition, there is recent evidence for a superposed M star in this system (Hammer, Le Fèvre, & Proust 1991; see also below). In the case of 3C 356, another well-studied object (Eales & Rawlings 1990; Eisenhardt & Chokshi 1990), it is clear that the “alignment effect” is morphologically distinct from that seen in most other radio galaxies, with a detached red lump several arcseconds away rather than a continuous smooth component extending out from the central object. The dynamical argument for this detached component not being a mature stellar population is correspondingly weaker. Even the more broadly based Eisenhardt & Chokshi (1990) study was nevertheless, in their words, “biased towards galaxies known to have extended asymmetric R-band and [O II] 3727 or Lyman  $\alpha$  emission.”

The present study was undertaken to examine the optical and infrared morphologies of distant radio galaxies in a systematic way. In this initial investigation we decided to limit our attention to moderate redshifts ( $z \approx 1$ ) so that (a) the objects are relatively bright and (b) a “statistically complete” sample could be observed. Our sample lies above the apparent onset of alignment effect at  $z = 0.8$  (McCarthy et al. 1987a), and we suspect that the radio galaxies at higher redshifts  $z > 2$  are qualitatively similar to those in the present sample at  $z = 1$ , though this is at present a conjecture (discussed further below). We have used a homogeneous set of optical and infrared line and continuum images of a well-defined sample of 13 3C radio galaxies with  $0.8 < z < 1.3$  that should be unbiased with respect to the properties of powerful radio galaxies as found in the 3C catalog at  $z \approx 1$ . Furthermore, we have attempted to carry out a quantitative and objective analysis of the morphologies of these galaxies as a function of wavelength in order to constrain the spectral energy distributions of the various morphological components and, in particular, to determine the contribution in the infrared of the “aligned” component that dominates at

short wavelengths. We find that the observations generally provide strong support for the basic old galaxy interpretation of high-redshift radio galaxies.

The organization of the paper is as follows: In the next section we describe the sample, our observations of it, and the reduction of our data. We then present a qualitative overview of the multicolor data, drawing attention to the basic features which are explored later in the paper. Next we develop and apply quantitative measures of the morphology at optical and infrared wavelengths, and argue that the morphologies of individual objects are entirely consistent with the old galaxy interpretation of these objects. We then turn to examine the global correlations between various radio galaxy properties that we could expect to find within the sample. We finally summarize the paper. Where required to calculate sizes and luminosities, we have assumed a Hubble constant of  $H_0 = 50 \text{ km s}^{-1} \text{ Mpc}^{-1}$  and  $q_0 = 0.5$ .

## 2. OBSERVATIONS

### 2.1. Sample Selection

The 13 radio galaxies observed here are selected from the complete 3C sample of Laing, Riley, & Longair (1983) updated with new redshifts from Spinrad et al. (1985). The radio galaxies were required to have  $0.8 < z < 1.3$ ,  $\delta < 55^\circ$ , and  $|b| > 15^\circ$ . 3C 263.1 at  $z = 0.824$  was accidentally omitted from the program because its redshift was listed in Laing et al. (1983) as  $z = 0.36$ . The primary selection criterion is thus radio luminosity coupled with the identification not having been classified as a “quasar.” The sample so defined is completely identified, and redshifts have been obtained for all identifications, so no objects are excluded on the basis of optical/infrared luminosity, color or morphology.

Images of these objects have been obtained over the last few years with all of the major optical/infrared telescopes of Mauna Kea.

### 2.2. Optical Imaging Observations and Reduction

In the initial phase of this project (reported by Stockton & Lilly 1988), CCD images of each galaxy were obtained in a narrow-band filter ( $\Delta\lambda = 50 \text{ \AA}$  in the rest frame) centered close to the redshifted [O II]  $\lambda 3727$  emission line and in two intermediate-band filters ( $\Delta\lambda = 200 \text{ \AA}$  in the rest frame) designed to exclude this emission line and to be located at around 4200 and 3500  $\text{\AA}$  in the rest frame. These were intended to be dominated by continuum emission above and below the 4000  $\text{\AA}$  feature in the galaxy spectrum. In a couple of cases (notably 3C 352) the shorter wavelength filter was contaminated with [O II]  $\lambda 2723$  emission, and in the case of 2C 266 (at the highest redshift in the sample), the longer wavelength continuum filter straddled the 4000  $\text{\AA}$  break rather than being clearly above it.

The observations were made with a Texas Instruments CCD detector ( $500 \times 500$ ) during runs on the University of Hawaii 2.2 m telescope and on the Canada-France-Hawaii 3.6 m telescope (CFHT) in 1986 June, 1987 July, and 1987 February. In each case, the detector was mounted at the Cassegrain focus behind focal-reducing optics which yielded image scales of  $0.40 \text{ pixel}^{-1}$  on the 2.2 m telescope and  $0.32 \text{ pixel}^{-1}$  on the CFHT. Photometric calibration was achieved through observations of spectrophotometric standards from the list of Oke & Gunn (1983). Reduction of these CCD images followed standard procedures using dome-flat exposures obtained immediately following each observation.

TABLE 1  
LOG OF OBSERVATIONS

3C	Filter	$\lambda_0$ (Å)	UT Date	Telescope	Device	Exposure(s)	Point-Spread Function
65.....	V	...	1987 Jun 19	CFHT	RCA2	1200	1.1
	SC	7515	1987 Feb 3	UH88	TI	1800	1.9
	[O II]	8115	1987 Feb 3	UH88	TI	3600	1.9
	LC	8784	1987 Feb 4	UH88	TI	3600	1.9
	H	...	1990 Sep 2	CFHT	NICMOS	4800	0.9
217.....	B	...	1990 May 20, 21	UH88	NSF1	8400	1.3
	SC	6535	1987 Feb 3	UH88	TI	1800	1.6
	[O II]	7078	1987 Feb 3	UH88	TI	3600	1.6
	LC	8300	1987 Feb 3	UH88	TI	3600	1.6
	K	...	1990 Mar 25	IRTF	PCAM	6960	1.0
	K	...	1990 Mar 31	UKIRT	IRCAM	7800	1.3
226.....	B	...	1990 May 22	UH88	NSF1	600	1.0
	SC	6535	1987 Feb 4	UH88	TI	1800	1.2
	[O II]	6800	1987 Feb 4	UH88	TI	3600	1.4
	LC	7515	1987 Feb 4	UH88	TI	3000	1.5
	K	...	1990 Mar 23	IRTF	PCAM	2400	1.1
252.....	V	...	1988 Jan 21	CFHT	RCA2	420	0.6
	SC	7515	1987 Feb 3	UH88	TI	1800	1.1
	[O II]	7851	1987 Feb 3	UH88	TI	3600	1.1
	LC	8784	1987 Feb 3	UH88	TI	4200	1.1
	H	...	1990 Mar 31	UKIRT	IRCAM	5400	1.3
265.....	V	...	1988 Jan 21	CFHT	RCA2	4800	1.1
	SC	6535	1986 Jan 6	UH88	TI	1200	1.1
	[O II]	6750	1986 Jan 6	UH88	TI	3600	1.1
	LC	7531	1986 Jun 6	UH88	TI	1200	1.1
	K	...	1990 Apr 1	UKIRT	IRCAM	2640	1.1
266.....	V	...	1988 Jan 20	CFHT	RCA2	3600	0.6
	SC	7531	1986 Jan 5	UH88	TI	1200	1.3
	[O II]	8479	1986 Jun 5	UH88	TI	3600	1.2
	LC	9100	1990 May 22	UH88	NSF1	7200	1.3
	H	...	1990 Mar 31	UKIRT	IRCAM	4860	1.0
267.....	V	...	1990 May 21	UH88	NSF1	3600	1.1
	SC	7531	1986 Jun 7	UH88	TI	1800	1.1
	[O II]	7955	1986 Jun 7	UH88	TI	3600	1.1
	LC	8784	1986 Jun 7	UH88	TI	1800	1.1
	H	...	1990 Mar 25	IRTF	PCAM	8640	1.1
	H	...	1990 Apr 1	UKIRT	IRCAM	5400	1.2
280.....	B	...	1990 May 19, 20	UH88	NSF1	10,800	1.0
	SC	6535	1986 Jul 2	CFHT	TI	960	1.0
	[O II]	7445	1986 Jul 2	CFHT	TI	1800	1.0
	LC	8295	1986 Jul 2	CFHT	TI	1800	1.0
	K	...	1990 Apr 1	UKIRT	IRCAM	3600	1.0
289.....	B	...	1990 May 19, 20	UH88	NSF1	12,000	1.6
	SC	6535	1986 Jul 3	CFHT	TI	1800	1.1
	[O II]	7338	1986 Jul 3	CFHT	TI	1200	1.1
	LC	8295	1986 Jul 3	CFHT	TI	1800	1.1
	K	...	1990 Mar 27	IRTF	PCAM	2400	1.2
324.....	V	...	1990 May 21	UH88	NSF1	4200	0.7
	SC	7531	1986 Jul 4	CFHT	TI	1800	1.1
	[O II]	8231	1986 Jul 4	CFHT	TI	1800	1.0
	LC	8784	1986 Jul 4	CFHT	TI	2700	1.1
	H	...	1990 Apr 1	UKIRT	IRCAM	6720	1.3
352.....	B	...	1990 May 19, 10	UH88	NSF1	10,800	1.2
	SC	6535	1986 Jun 6	UH88	TI	1800	1.5
	[O II]	6750	1986 Jun 6	UH88	TI	3600	1.6
	LC	7531	1986 Jun 6	UH88	TI	2400	1.7
	K	...	1990 Mar 25	IRTF	PCAM	7440	1.1

TABLE 1—Continued

3C	Filter	$\lambda_0$ (Å)	UT Date	Telescope	Device	Exposure(s)	Point-Spread Function
356.....	<i>B</i>	...	1987 May 30	CFHT	RCA2	1200	1.3
	SC	7531	1986 Jun 5	UH88	TI	2400	1.3
	[O II]	7755	1986 Jun 5	UH88	TI	3600	1.3
	LC	8784	1986 Jul 4	UH88	TI	2700	1.3
	<i>K</i>	...	1990 Mar 27	IRTF	PCAM	5040	1.3
368.....	<i>B</i>	...	1987 Jun 19	CFHT	RCA2	2400	1.0
	SC	7531	1986 Jul 2	CFHT	TI	1800	1.0
	[O II]	7955	1986 Jul 2	CFHT	TI	1800	1.2
	LC	8784	1986 Jul 2	CFHT	TI	2400	1.2
	<i>H</i>	...	1990 Mar 31	UKIRT	IRCAM	4200	1.3
	<i>K</i>	...	1990 Mar 27	UKIRT	IRCAM	4560	1.3

A linear combination of the two intermediate-band continuum filters on either side of the [O II]  $\lambda 3727$  line was used to generate a continuum image which was subtracted from the narrow-band image to give a line-only [O II]  $\lambda 3727$  image.

Additional optical images were subsequently obtained with the University of Hawaii 2.2 m telescope during a run in 1990 March with a TI 800  $\times$  800 detector at 0".26 pixel<sup>-1</sup>. In order to obtain data at approximately the same rest wavelength of around 2500 Å, images were taken in the *B* band for galaxies with redshifts less than about 1.1 and in the *V* band for galaxies with higher redshifts. Observations of Landolt (1982) standards were used to calibrate these broad-band data. The higher background flux permitted the use of short exposures between which the telescope was moved 10"–20" in a mosaic pattern. This allowed sky-flattening procedures to be used in which the data were used to define the flat-field pattern through the standard use of median filtering techniques.

Finally, we have utilized several of the *B* and *V* images of some of the program objects that have previously been published elsewhere (Le Fèvre, Hammer, & Jones 1988; Le Fèvre & Hammer 1988; Hammer & Le Fèvre 1990). In Table 1 we list the telescope/detector combination used for the observations, the FWHM of the point-spread function, the exposure time, and the central wavelengths (in the observed frame) of nonstandard filters used for the observations.

### 2.3. Infrared Imaging Observations and Reduction

Infrared images of these galaxies were obtained with the NASA 3.0 m Infrared Telescope Facility (IRTF) and the 3.8 m United Kingdom Infrared Telescope during 1990 March. In both cases, an InSb 58  $\times$  62 SBRC array detector was used at the Cassegrain focus at plate scales of 0".35 pixel<sup>-1</sup> and 0".62 pixel<sup>-1</sup>, respectively. 3C 65 was observed with the CFHT in 1990 September using a HgCdTe 256  $\times$  256 Rockwell array at 0".29 pixel<sup>-1</sup>. In an attempt to minimize the effects of strong emission lines on our broad-band observations, the radio galaxies with  $z < 1.10$  were observed in *K* and the remainder in *H*, thereby avoiding the strong [S III]  $\lambda\lambda 9069, 9059$  lines. The galaxies at lower redshifts were thus observed at around 1.2  $\mu\text{m}$  in the rest frame, while the ones at higher redshift were observed at shorter rest wavelengths around 7000 Å.

The reduction of the infrared images employed statistical techniques to determine the instrumental response and to flatten the background. Many short exposures (2–4 minutes) were taken, between which the telescope was moved in a complex sequence around a rectilinear mosaic pattern comprising 25 positions. The minimum spacing in this mosaic

pattern was dictated by the field of view of the detector array, and was 7".5 at CFHT, 5" at UKIRT, and 3" at IRTF. Nevertheless, the typical displacement between adjacent frames in the observing sequence was much larger. After subtraction of a dark frame of equal exposure and application of the linearizing algorithm to take out the intrinsic nonlinearity of the detectors, a background for each frame was constructed through the median averaging of normalized versions of the four preceding and four following images. A scaled version of this background was then subtracted from the image. Photometric variations across the chip were corrected by the division into each frame of a "bright-sky" flat, although in the case of UKIRT data this final step had a negligible effect.

The individual images were then coregistered and co-added as follows: UKIRT has an automated offsetting routine that coordinates motions of the telescope and of the *x-y* stage of the TV guider. The UKIRT data were coregistered using the offsets measured on the infrared detector when a standard star was observed through the same sequence of offsets, thereby removing any hysteresis effects in the positioning of the *x-y* stage. Examination of those fields that contained one or more field stars showed that the coregistration process produced no significant degradation of the point-spread function. The IRTF does not have this facility at present, at least in part because the telescope tracks and offsets with high accuracy. The objects observed with IRTF were sufficiently bright that small adjustments to the commanded offset pattern (to remove the effects of telescope drift over the hour or so of the observation sequence) could, however, be readily determined.

Finally, the sky background was further refined by calculating the modal value of pixels in regions out to 20"–40" away from the radio galaxy. Photometric calibration of all the infrared images was based on the standard stars of Elias et al. (1982). Details of these observations are also listed in Table 1.

### 2.4. Combining the Data

The calibrated images in each wave band were transformed through rotations and scalings to have the same orientation (within a degree of north = top, east = left) and a constant plate scale of 0".200 pixel<sup>-1</sup>. The point-spread function (PSF) for each image was determined from stellar images on the final images where possible. For several of the infrared images obtained at IRTF, and for some of the UKIRT ones, no stars were visible within the restricted field of view of the final image. In these cases it was assumed that the PSF was the same as in other images taken at a similar time. For each object, a simple single Gaussian smoothing was applied to the images, so that

stellar images on the “co-smoothed” images would have a constant FWHM, defined by the “worst” image of the original “unsmoothed” images. With five images for each galaxy, the standard PSFs to which the images were smoothed are listed in Table 3 and were generally in the range  $1''.0$ – $1''.5$ .

Primary photometric and morphological analysis was carried out on  $15'' \times 15''$  subimages extracted from both the unsmoothed and the co-smoothed images and centered on the peak of the infrared emission. Montages of the unsmoothed images in each wave band for each radio galaxy are shown in Figures 2a–2m (except for 3C 265, where the images are  $30''$  to a side to accommodate the very large-scale extended structure). These have been plotted with contours at logarithmic intervals of surface brightness (at a factor of 1.41, so that two contours represent a factor of 2 in surface brightness). It should be noted that this results in rather fewer contours than are typically represented on linear plots, but has the advantage that the relative colors and magnitudes of different components can be most easily seen. The level of the lowest contour on each plot is indicated in AB magnitudes per square arcsecond.

Those images of the radio galaxies that have equal numbers of contours thus have comparable dynamic range. The images show that, by and large, the goal of having roughly equal dynamic range in all wave bands for a given galaxy was achieved. However, the capabilities of infrared imaging on very red, quiescent, objects at high redshifts is well demonstrated by

our superb  $H$ -band image of 3C 65, which is far superior to our optical data.

Aperture magnitudes on the AB system measured through a circular  $4''$  aperture are listed in Table 2, together with the Galactic latitude and assumed  $E_{B-V}$ —usually very small. It should be noted that these are in no way meant to be “total” magnitudes, and are mainly intended to serve as the basis of the construction of spectral energy distributions over a wide baseline in wavelength. The use of isophotal magnitudes or of schemes whereby the aperture is tailored to the morphology of individual objects would have defeated the purpose of this investigation. These magnitudes have been corrected for Galactic reddening using the  $E_{B-V}$  maps of Burstein & Heiles (1982). The AB magnitudes in the standard  $B$ ,  $V$ ,  $H$ , or  $K$  bands may be transformed back to the standard  $\alpha$  Lyrae photometric system by the addition of the following constants: 0.17, 0.00,  $-1.43$ , and  $-1.91$  for  $B$ ,  $V$ ,  $H$ , and  $K$ , respectively.

Good agreement was found between the new infrared measurements and the single-element aperture photometry of Lilly & Longair (1984). We have constructed synthetic aperture magnitudes from the two-dimensional infrared data through the same apertures used by Lilly & Longair (1984) and have compared these with the Lilly & Longair values in Figure 3. The rms magnitude difference is 0.26 mag, consistent with the statistical uncertainties, which are typically 20% for each data set. The uncertainty in the array magnitudes in these large

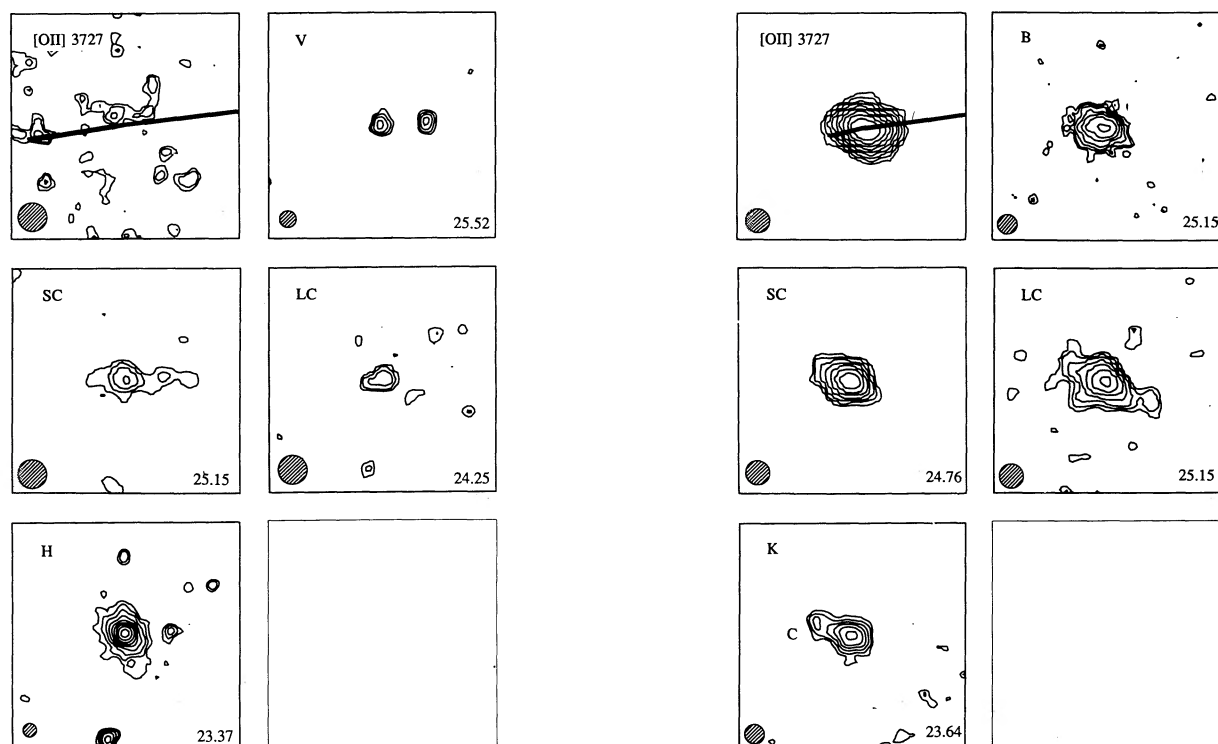


FIG. 2a

FIG. 2b

FIG. 2.—(a–m) Montages of the unsmoothed multicolor images of each of the 13 3C radio galaxies observed in this program. The images are  $15''$  square (except 3C 265, which is  $30''$  square), and are accurately coregistered. Orientation is within  $1^\circ$ – $2^\circ$  of NSEW, with north at the top and east at the left. Contours are plotted in logarithmic surface brightness (at root 2 intervals in surface brightness). Images are identified by standard filter passbands except for LC and SC, which stand for the intermediate-band filters located above and below the  $4000 \text{ \AA}$  spectral feature. The small disk represents the FWHM of the seeing point-spread function. The number indicates the level of the lowest contour in AB mag arcsec $^{-2}$ . The radio jet axes are sketched on the [O II]  $\lambda 3727$  images, and red companions, discussed in the text, are marked by C. (a) 3C 65 ( $z = 1.176$ ); (b) 3C 217 ( $z = 0.898$ ); (c) 3C 226 ( $z = 0.823$ ); (d) 3C 252 ( $z = 1.103$ ); (e) 3C 265 ( $z = 0.811$ ); (f) 3C 266 ( $z = 1.275$ ); (g) 3C 267 ( $z = 1.140$ ); (h) 3C 280 ( $z = 0.996$ ); (i) 3C 289 ( $z = 0.967$ ); (j) 3C 324 ( $z = 1.206$ ); (k) 3C 352 ( $z = 0.806$ ); (l) 3C 356 ( $z = 1.079$ ); (m) 3C 368 ( $z = 1.132$ ).

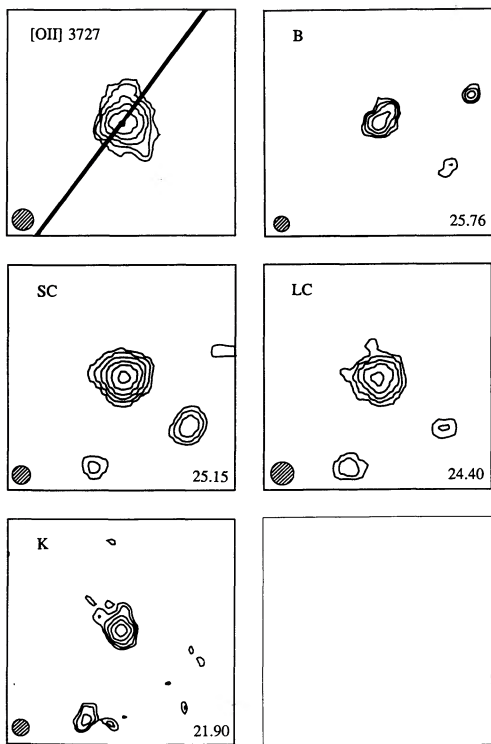


FIG. 2c

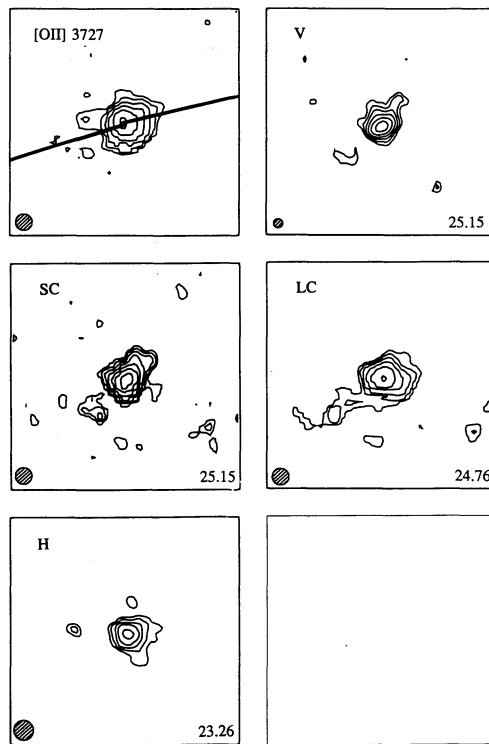


FIG. 2d

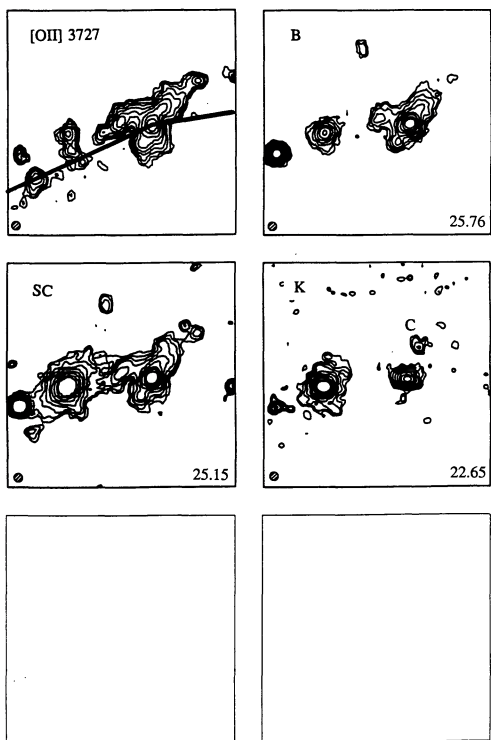


FIG. 2e

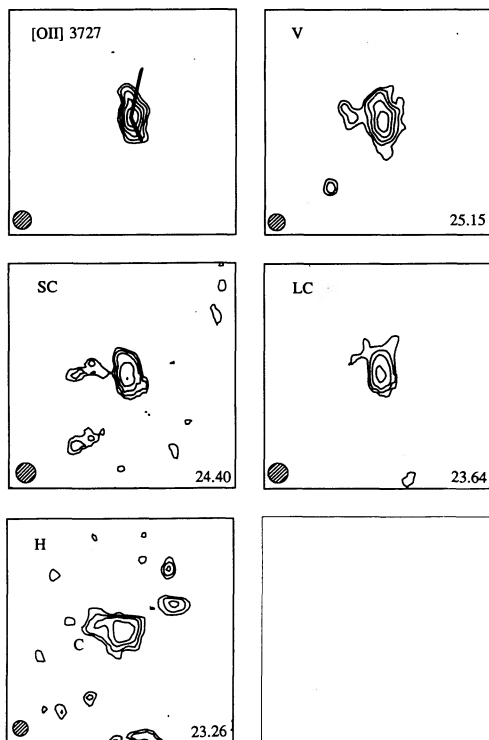


FIG. 2f

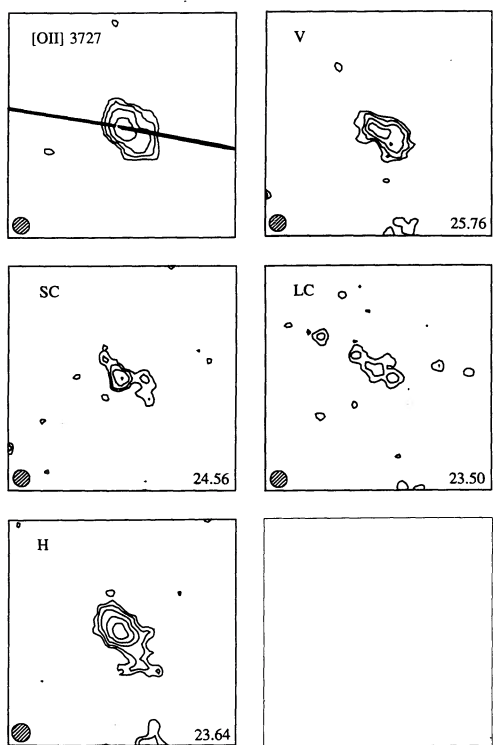


FIG. 2g

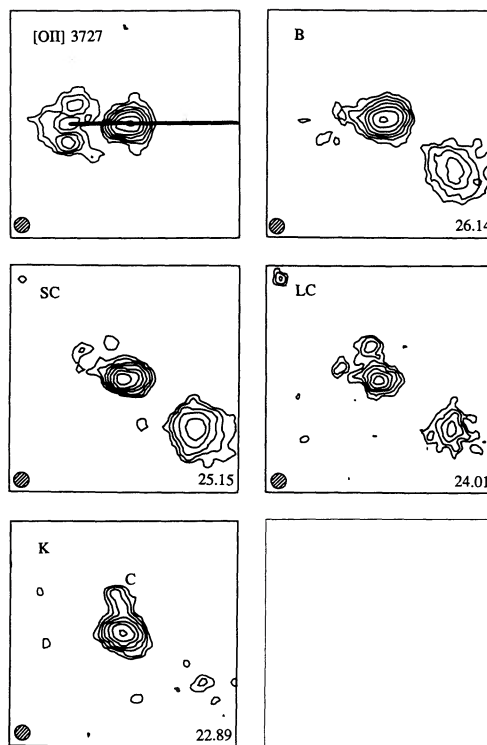


FIG. 2h

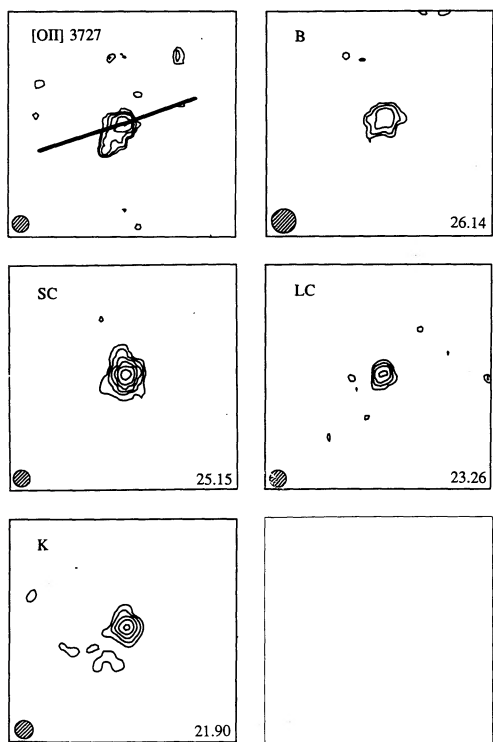


FIG. 2i

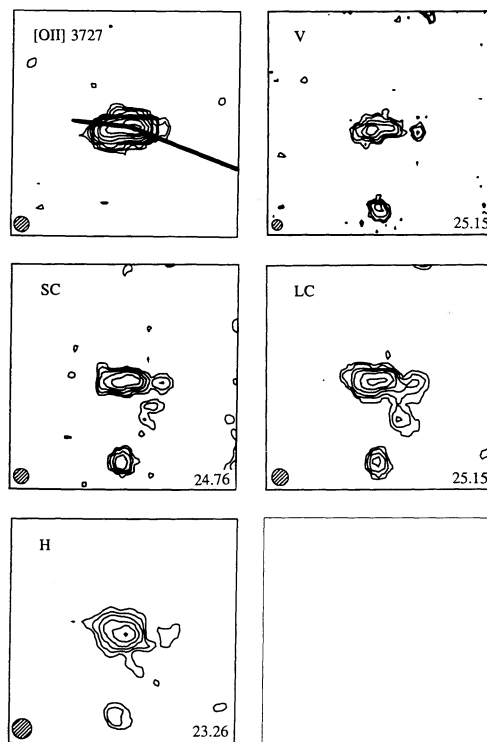


FIG. 2j

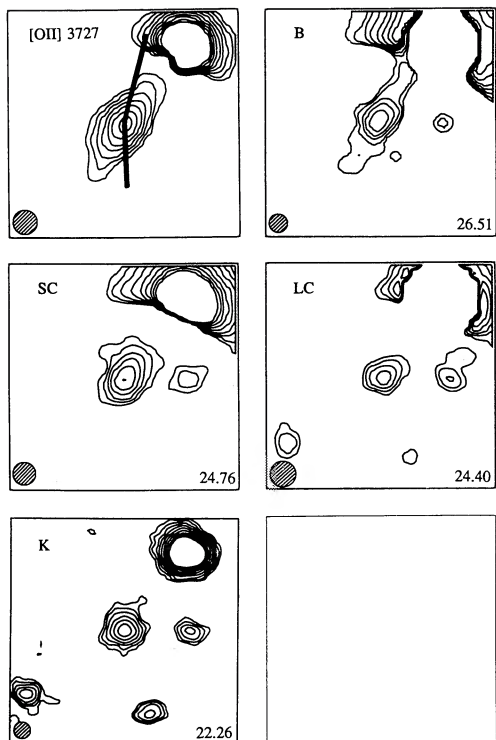


FIG. 2k

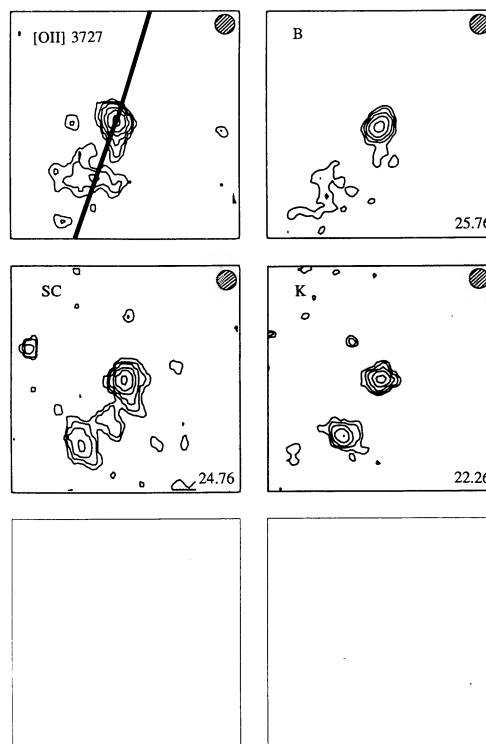


FIG. 2l

synthetic apertures is dominated by uncertainty in the determination of the background level.

### 3. QUALITATIVE OVERVIEW

Visual inspection of the images in Figure 2 suggests that the infrared images are generally more compact and symmetric about the peak in the surface brightness distribution. Some of the infrared images appear almost completely round despite striking elongations at shorter wavelengths, and, given the number of contours in each image, it is evident that this is not simply a dynamic range effect. A particularly good example of this is given by 3C 352 (see Fig. 2k). On the other hand, several objects do appear to be elongated in the infrared along the axes defined by the shorter wavelength light. Examples of these include 3C 267, 3C 280, and 3C 324, as well as the well-studied 3C 368 (see also Chambers et al. 1988a; Djorgovski et al. 1991). Nevertheless, even in these objects, the infrared emission generally appears to be more centrally concentrated, consistent with the idea that the elongated component is simply the “tail” of the component that dominates at shorter wavelengths. For instance, careful study of 3C 324, which appears to show a convincing case of alignment, reveals that the peak of emission shifts between the optical and infrared images: the red western component is brightest at *K*, and the much bluer eastern component is brightest at *B*.

Finally, many objects show evidence of companions or extensions in the infrared in directions well away from the radio source axis. These are also visible in the longer wavelength optical continuum images around 4000 Å, but are fainter or have disappeared in the rest-frame 2500 Å and [O II] λ3727 images. We believe that these extensions and condensations represent early-type galaxy companions to the radio galaxies that have probably triggered the radio activity in a

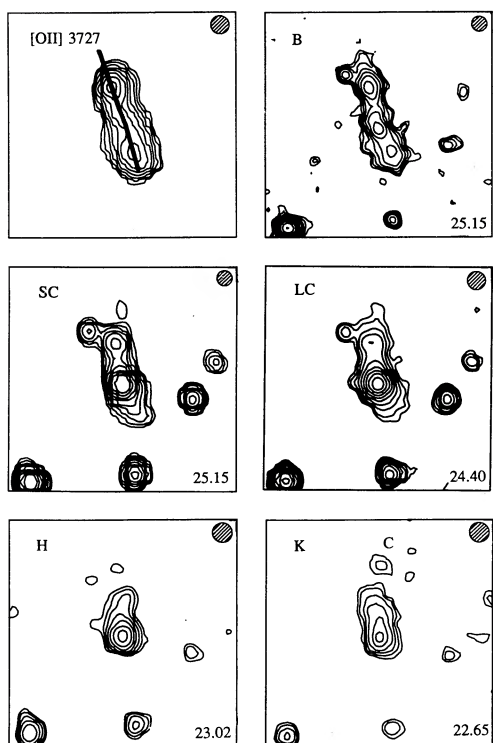


FIG. 2m

TABLE 2  
SPECTRAL ENERGY DISTRIBUTIONS

3C	$z$	$b$	$E_{B-V}$	AB MAGNITUDES			
				2500 Å	SC	LC	1 $\mu\text{m}$
65	1.176	-20°	0.04	23.38 (V)	22.15	21.73	19.43 (H)
217	0.898	43	0.00	21.93 (B)	21.68	21.14	20.14 (K)
226	0.823	43	0.00	22.99 (B)	21.47	20.94	18.83 (K)
252	1.103	67	0.00	21.93 (V)	21.34	21.17	20.15 (H)
265	0.811	75	0.00	20.77 (B)	19.98	...	18.43 (K)
266	1.275	64	0.00	21.82 (V)	21.42	20.81	20.09 (H)
267	1.140	70	0.00	22.86 (V)	21.98	20.92	20.34 (H)
280	0.996	70	0.00	22.75 (B)	21.44	20.79	19.10 (K)
289	0.967	65	0.00	23.44 (B)	21.92	20.88	19.02 (K)
324	1.206	49	0.03	22.47 (V)	21.56	21.60	19.75 (K)
352	0.806	36	0.03	22.92 (B)	21.07	21.49	19.10 (K)
356	1.079	34	0.03	22.70 (B)	21.43	20.39	19.53 (K)
368	1.132	15	0.17	20.57 (B)	20.41	19.82	19.18 (K)

close encounter. Good examples of this phenomenon, which we discuss in more detail below, are given by 3C 265, 3C 266, and 3C 280.

#### 4. QUANTITATIVE MORPHOLOGICAL ANALYSIS

A main motivation for this study was the desire to go beyond a simple qualitative description of the images and obtain quantitative measurements of the morphology of the radio galaxies in order to provide a crude determination of the relative contributions of distinct morphological components in each wave band.

##### 4.1. A Quantitative Measure of Asymmetry

It is straightforward to define a centroid, position angle, and ellipticity for each image from a combination of the zeroth-, first-, and second-order moments,  $\Sigma\mu$ ,  $\Sigma x\mu$ ,  $\Sigma y\mu$ ,  $\Sigma xy\mu$ ,  $\Sigma x^2\mu$ , and  $\Sigma y^2\mu$ , where  $\mu$  is the sky-subtracted surface brightness distribution of the image. These summations were carried out over a circular aperture 4" in diameter for all the images, and

the derived quantities are listed in Table 3, together with the FWHM to which the images were co-smoothed. The choice of 4" diameter for the aperture used in deriving these parameters represents a trade-off between the desire to include as much as possible of the galaxy light and the increased noise and greater chance of contamination by unrelated objects. The analysis was repeated with a 6" diameter aperture, but this produced no substantial difference in the results. At these redshifts, a diameter of 4" corresponds to roughly the standard sampling radius  $\gamma$  (19.2 kpc radius) introduced by Gunn & Oke (1975). In only one case, 3C 265, is the extended structure outside the 4" aperture oriented significantly differently. It should also be noted that the 3C 356 system consists of a pair of objects separated by 4".5 along the radio axis (see below). We have listed in Table 3 the radio source position angle (measured east from north) as determined from published 5 GHz radio maps (Jenkins, Pooley, & Riley 1977 and references therein; Pedely et al. 1989) by simply constructing a line connecting the two radio lobes. The optical/infrared P.A. information is given relative to the radio in the sense  $\Delta\text{P.A.} = \text{P.A.}(\text{optical}) - \text{P.A.}(\text{radio})$ . In this initial analysis, no attempt was made to remove nearby objects from the optical and infrared images unless they were clearly unrelated to the radio galaxy, as is the case with the bright star near 3C 352.

Describing these objects by a single moment parameter clearly does not do justice to their often complex morphologies. Nevertheless, we believe that it offers the best possibility for the objective assessment of the relative contributions of different morphological components at different wavelengths. As an example of possible limitations in this approach, we note that the V-band images of 3C 65 and 3C 266 have identical ellipticities (on their respective "co-smoothed" images) but quite distinct morphologies (on the unsmoothed images of Fig. 2). This arises because of the heavy smoothing applied to the 3C 65 images which has brought the companion into the edge of the aperture used to determine the moment parameters, where it has a large effect on the second moment.

The ellipticity of the images as a function of the difference in position angle with respect to that of the radio axis,  $|\Delta\text{P.A.}|$ , has been plotted for all the galaxies in the sample in Figure 4 in the  $[\text{O II}] \lambda 3727$  image, in the roughly 2500 Å continuum band (observed in B or V), and in the roughly 1  $\mu\text{m}$  continuum band (observed in H or K). The "alignment effect" of McCarthy et al. (1987b) and Chambers et al. (1987) is clearly visible in the

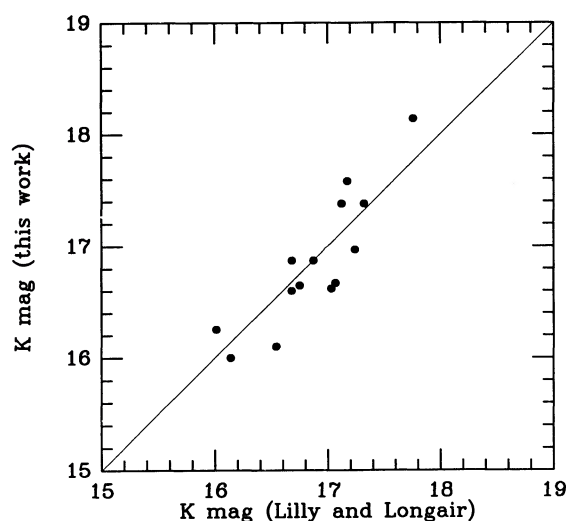


FIG. 3.—Comparison of single-element aperture photometry from Lilly & Longair (1984) and aperture photometry (through the same aperture) constructed from the present two-dimensional array data. Where the observations were carried out in the H band, they have been converted to K using  $(H - K) = 1.0$ .

TABLE 3  
 ALIGNMENT PARAMETERS

3C	POINT-SPREAD FUNCTION	2500 Å		[O II] $\lambda$ 3727		1 $\mu$ m		RADIO	
		$\epsilon$	$\Delta$ P.A.	$\epsilon$	$\Delta$ P.A.	$\epsilon$	$\Delta$ P.A.	P.A.	SIZE
65	1.9	0.12	-19.5	0.25	-18.2	0.06	-64.4	95°	16"
217	1.6	0.15	-25.6	0.18	-24.3	0.13	-26.5	98	12
226	1.5	0.12	-2.5	0.02	39.3	0.14	67.8	146	35
252	1.3	0.09	20.8	0.05	22.2	0.01	4.7	106	60
265	1.1	0.10	19.3	0.15	67.3	0.12	-22.8	107	78
266	1.3	0.12	9.6	0.44	5.9	0.19	70.1	7	4
267	1.2	0.32	-20.5	0.17	-39.4	0.33	-33.5	80	38
280	1.0	0.27	18.1	0.10	8.0	0.13	-29.5	91	12
289	1.7	0.14	44.8	0.17	37.5	0.08	48.4	109	10
324	1.3	0.24	25.2	0.36	19.5	0.11	-2.1	77	10
352	1.7	0.21	-29.2	0.20	-22.8	0.06	-12.2	176	10
356	1.3	0.13	-3.0	0.19	30.7	0.05	58.1	171	71
368	1.3	0.43	3.1	0.41	1.1	0.31	-9.3	18	8

[O II]  $\lambda$ 3727 and 2500 Å panels of this figure. Essentially all of the radio galaxies have position angles at these wavelengths that are within 40° of the radio source axis, with many within 20°. The sole exception is the [O II]  $\lambda$ 3727 image of 3C 265, which, as remarked above, shows a much closer alignment on scales outside the 4" aperture (see Fig. 2). There is clearly also a

trend for the most elongated images to be the most closely aligned with the radio axis.

In contrast, the position angles determined in an identical way from the infrared images show a wide spread with regard to the radio source axis and no tendency for the more elongated images to be most preferentially aligned. *In the infrared wave band there is therefore little if any of the global "alignment effect" so strongly shown by the optical images*, at least in this well-defined sample at  $0.8 < z < 1.3$ . Examination of those infrared images which are elongated but misaligned with respect to the radio axis shows that the high values of the ellipticity parameter are generally produced by small, rather red, companion galaxies located within or on the edge of the 4" aperture. Inspection of these images shows that the main galaxy component either is round or is weakly elongated along the axis defined by the radio source and optical emission. We explore the nature of these companions more extensively below.

In order to quantify the degree of asymmetry in our images, we have used additional moment parameters. The following considerations guided our choice: (a) they are usually confined to within a few arcseconds of the nominal center of the galaxy—this being most true in the case of those components which are most demonstrably elongated and which hence cannot be dynamically old; (b) we wanted parameters that would be as insensitive as possible to errors in the PSF used in the co-smoothing operation and to errors in the determination of the sky background level.

We therefore defined a quadrupole alignment moment,  $S = \Sigma(x'^2 - y'^2)\mu/\Sigma\mu$ . In this summation,  $x'$  and  $y'$  are transformed coordinates such that the  $x'$  axis is some "preferred" axis, and the  $y'$  axis is perpendicular to it. As before, the summation was carried out over a 4" diameter circular aperture centered on the peak of the infrared image. We also defined a second parameter,  $T = \Sigma(|x'| - |y'|)\mu/\Sigma\mu$ , which weights the outer parts of the images less heavily, but found no significant differences in our analysis when we employed this parameter. The remainder of our discussion is based on the  $S$ -parameter.

The parameter  $S$  is clearly zero for any circularly symmetric image and zero for an image aligned at 45° to the preferred axis, positive for an image aligned along the preferred axis, and negative for an image aligned orthogonally to this direction. If an image is composed of two components A and B which individually have  $S$ -values of  $S_A$  and  $S_B$ , then it is easy to show

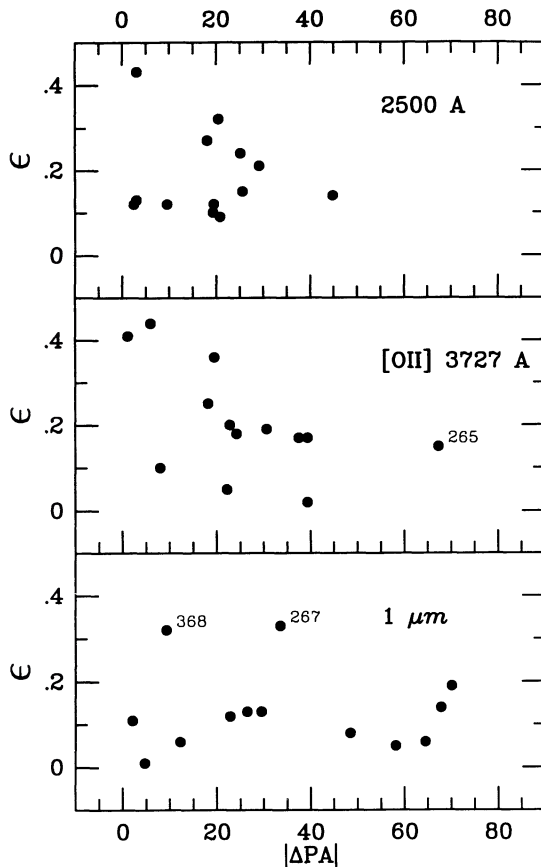


FIG. 4.—Ellipticity parameter  $\epsilon$  plotted against the absolute value of the difference in position angle with respect to that of the radio source axis for the continuum image at approximately rest-frame 2500 Å, for the [O II]  $\lambda$ 3727 emission line, and for the infrared continuum at approximately rest-frame 1  $\mu$ m.

that the wavelength-dependent value of  $S(\lambda)$  for the composite image is simply given by  $S(\lambda) = f_A(\lambda)S_A + [1 - f_A(\lambda)]S_B$ , where  $f_A(\lambda)$  is the fraction of the total light (within the aperture) that is contributed by the A component. Of particular interest is the case where A is a strongly aligned component whose position angle defines the preferred axis, and B is a circularly symmetric component. In this case,  $S_B = 0$ , so that  $S(\lambda) = f_A(\lambda)S_A$ .

In analyzing our images, we have arbitrarily taken the shortest wavelength continuum image (at approximately 2500 Å in the rest frame) to define an “active” component and have determined the position angle of the preferred axis and the value of  $S_A$  from this image. Choice of the [O II] λ3727 image as the defining image for  $S_A$  did not make much difference to the overall results, reflecting the fact that the 2500 Å and [O II] λ3727 images are usually similar. We have assumed that the only other component present is a circularly symmetric component, taken to have  $S_B = 0$ . For each of the remaining images, we can therefore determine the relative contributions of these two morphological components by measuring  $S(\lambda)$  and thus determining  $f_A(\lambda) = S(\lambda)/S_A$ . It should be stressed that this simple morphological decomposition *may have no physical basis*. It is used to estimate the fraction of the light in the long-wavelength images (i.e., the infrared *H* or *K* images) that *must* come from a symmetric component, assuming that the asymmetric component has the morphology defined by the shortest wavelength image. As discussed above, this provides the most straightforward test of the idea that the *K*-band light is dominated by a mature relaxed galaxy, *since as one moves to longer wavelengths the value of  $S(\lambda)$  should progressively decrease toward zero*. Clearly, if the short-wavelength images themselves contain a significant contribution from the symmetric component, then the contribution of this component at longer wavelengths will also have been correspondingly underestimated.

Once  $f_A(\lambda)$  and the overall spectral energy distribution within the aperture is determined for a given galaxy as a function of wavelength, it is straightforward to produce spectral energy distributions for the aligned and symmetric components separately. It should be stressed again that these may not be physically meaningful: in particular, our method of analysis sets the flux density of the symmetric component to zero at the shortest wavelengths. However, these curves will serve to illustrate how the aligned parts of the galaxies are bluer than the central symmetric parts.

The individual measurements of  $S_A$  and  $S(\lambda)$  are of course dependent on the point-spread function, being smaller for more highly smoothed images. However, provided that the seeing is the same for all the images of a particular galaxy, as we have attempted to ensure through the co-smoothing operation, the ratio,  $f_A(\lambda)$ , should be unaffected. This has been veri-

fied using different smoothings of the two-component model galaxies discussed in § 1. The value of  $S_A$  for the linear component in the model varies as (30.4, 24.8, 21.0, 19.1) for seeing of (0.5, 1.0, 1.5, 2.0), but the corresponding values of  $f_A$  are almost constant at (0.206, 0.200, 0.197, 0.196). If an error in the co-smoothing process resulted in a discrepancy of 20% in the effective seeing for the different images, this would, however, translate to an error of 10% in the value of  $f_A$ .

We have estimated the statistical uncertainties in the derived values of  $f_A(\lambda)$  in two ways. First, we have constructed a suite of simulated galaxies using the de Vaucouleurs galaxy model with a linear active component that was described in § 1 with  $f_A = 0.2$ . To these we have added noise with the approximate characteristics of the noise encountered in our actual images (see selected examples in Fig. 1, *lower panel*). From these simulated data, we find an rms error in  $f_A$  of 0.1, and find that this is largely independent of the amount of smoothing applied to the image (over the range 0.5–2.0). Second, we have examined the moment parameters derived from multiple images that are available for some objects, and find that these agree to within about 0.1 in  $f_A$ . For simplicity we take 0.1 as a reasonable estimate of the uncertainty of  $f_A$ . In passing, the uncertainty in the position-angle determination for the angle determination of the  $f_A = 0.2$  model (representative of our infrared data) was 5° for 1" seeing and about 10° for 2" seeing, but would be larger for objects with an even smaller contribution from the aligned component. This may account for some of the spread of P.A. measurements in the infrared seen in Figure 4, but we suspect that the dominant effect is that of nearby companions at “random” relative P.A.

The morphological decomposition obviously works best for (a) those objects that are most elongated and “aligned” so that  $S_A$  is large and small random errors do not dominate the change of morphology with wavelength, and (b) those which do not have bright nearby companions that may distort the  $S(\lambda)$  values as a function of wavelength if the radio galaxy and companion have different spectral energy distributions. We have carried out this morphological decomposition analysis for 3C 65, 3C 265, 3C 280, 3C 324, and 3C 352. The values of  $S(\lambda)$  and  $f_A(\lambda)$  as a function of wavelength for these five galaxies are listed in Table 4, and the resulting two-component spectral energy distributions are shown in Figures 5a–5e. The remaining galaxies are less suited to this detailed individual analysis, usually because a bright infrared companion is producing an orthogonal alignment in the infrared and hence formally a negative value of  $f_A(\lambda)$ , or because the images are almost round in all wave bands, so that small uncertainties dominate the variation in  $f_A(\lambda)$ .

These spectral energy distributions (SEDs) clearly demonstrate that in these objects, *a substantial symmetric component*

TABLE 4  
MOMENT ANALYSIS

3C	2500 Å		SC		[O II] λ3727		LC		1 μm <sup>a</sup>	
	S	f <sub>A</sub>	S	f <sub>A</sub>	S	f <sub>A</sub>	S	f <sub>A</sub>	S	f <sub>A</sub>
65.....	3.89	1.00	3.77	0.97	0.55	0.14	2.01	0.52	-0.26	-0.07
265.....	4.02	1.00	2.22	0.55	-1.12	-0.15	...	...	0.39	0.10
280.....	10.48	1.00	5.89	0.56	5.02	0.48	2.88	0.27	0.04	0.00
324.....	10.69	1.00	9.95	0.93	11.77	1.10	8.57	0.80	2.44	0.22
352.....	7.04	1.00	5.29	0.75	6.99	0.99	1.93	0.27	1.27	0.18

<sup>a</sup>  $\tilde{f}_A(1 \mu\text{m}) = 0.08$ .

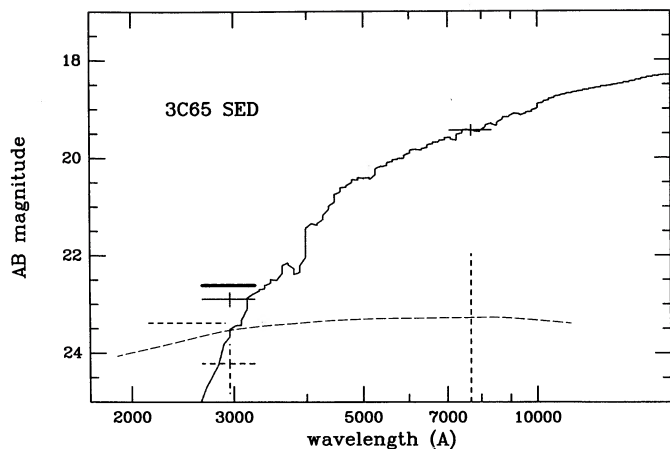


FIG. 5a

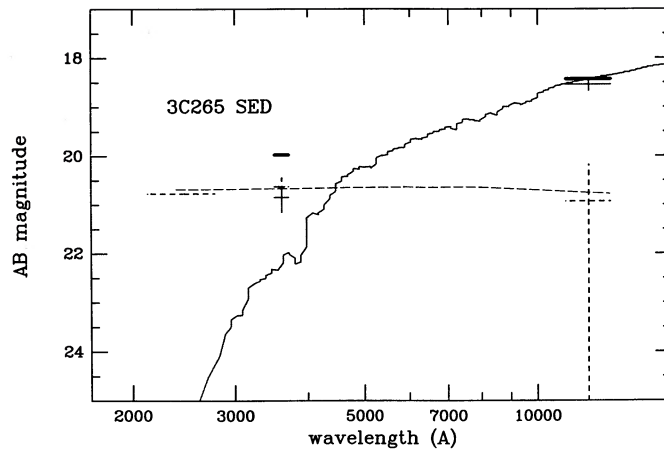


FIG. 5b

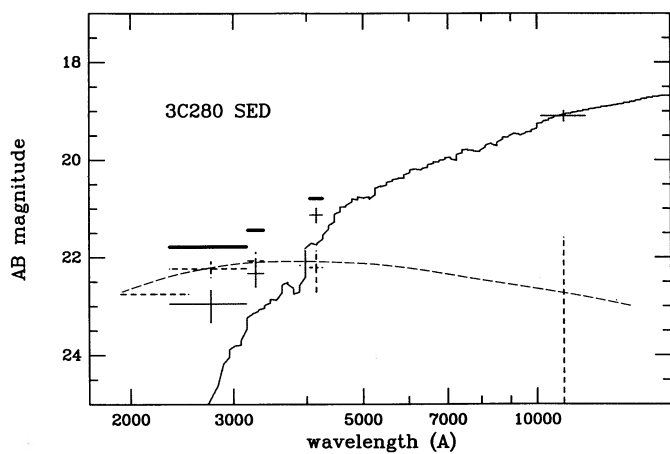


FIG. 5c

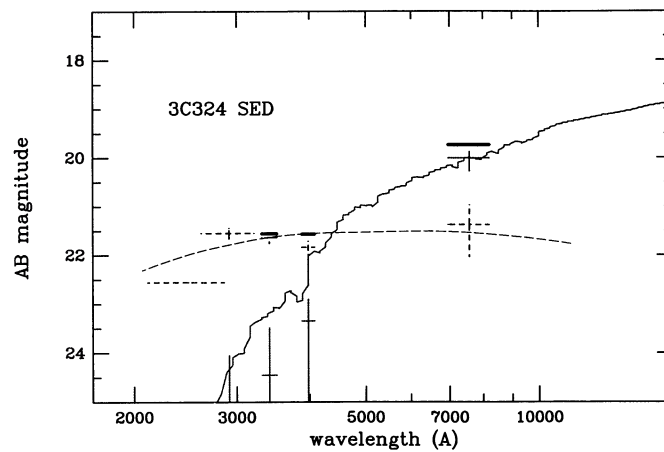


FIG. 5d

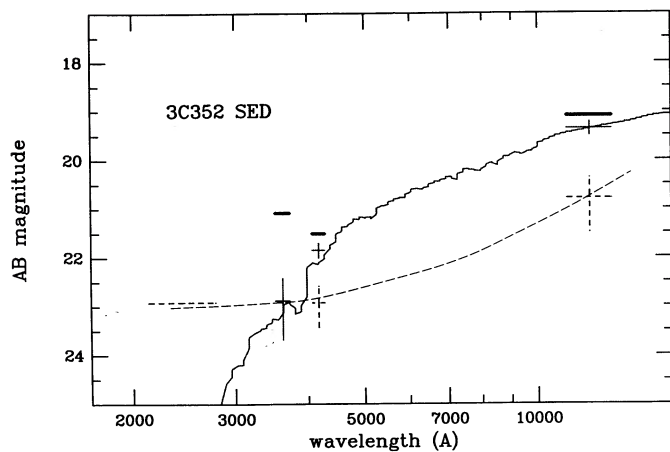


FIG. 5e

FIG. 5.—(a–e) Spectral energy distributions for the five galaxies for which a morphological decomposition was attempted (heavy horizontal lines). The horizontal width of lines indicates the approximate bandpass of each filter. Other lines represent the “asymmetric” (dashed line) and “symmetric” (continuous line) components based on the nonunique morphological decomposition described in the text. Vertical error bars are based on a 10% uncertainty in the  $f_{\lambda}(\lambda)$  parameter. For reference, the spectral energy distribution of a gE galaxy (Coleman et al. 1980) is shown passing through the “symmetric” point at long wavelengths, and a smooth continuum has been drawn by eye through the “asymmetric” component. Note that the 2500 Å continuum is assumed, in this analysis, to define the “asymmetric” component. The figures indicate that while this asymmetric aligned component dominates at very short wavelengths, it has a roughly flat spectral energy distribution in  $f_{\nu}$  and contributes only a small fraction of the infrared light. Continuum bands which were contaminated by [O II]  $\lambda 3727$  emission or were of very low quality have been omitted.

must be added to the short-wavelength images in order to match the observed morphologies in the infrared. This is of course exactly the result expected from the model in which all of these galaxies, regardless of their overall color, contain a mature massive galaxy that dominates the light at infrared wavelengths. For the five galaxies for which this detailed analysis was possible, the average contribution of the asymmetric “aligned” component to the infrared light is about 8%.

Mindful of the arbitrary and nonunique nature of the morphological decomposition, the SEDs in Figure 5 suggest that the active “aligned” component has a spectral energy distribution that is usually roughly flat,  $f_\nu = kv^0$ , over the 2500 Å to 1 μm interval, and suggest that the symmetric components may have a spectral energy distribution that is broadly similar to those of present-day gE galaxies. In order to aid the eye, we have sketched in by hand a smooth curve to represent the SED of the aligned component. A more sophisticated approach is not warranted, on account of the crudity of the morphological analysis. We note in passing that several objects (most notably 3C 280 and 3C 324) exhibit a turn-down in the SEDs of the decomposed “aligned” component at short wavelengths produced by a similar turn-down in the overall SED. A broadly flat SED in  $f_\nu$  is consistent with both a young starburst (e.g., Bruzual 1983) and the scattered light from an anisotropically emitting quasar nucleus.

On a more speculative note, we notice that the reddest “aligned” component in Figure 5 is that of 3C 352, which has a conspicuous misalignment with respect to the radio axis in Figure 2. If star formation is responsible for the blue aligned component, this could reflect an aging effect as the jet precesses to new orientations. This idea receives some support from the fact that other radio galaxies appear to have infrared extensions at slightly different P.A.s to the far-ultraviolet light (e.g., 3C 267, 3C 280, and 3C 324).

The effects of companions, etc., that led us not to analyze the remaining eight objects individually should, however, cancel out within the sample as a whole. We have therefore plotted in Figure 6 the values of  $S_A$  (defined as before from the shortest wavelength image) and  $S$  for the infrared image for all the galaxies in the sample. It may be seen that, as expected,  $S(\lambda)$  in the infrared is generally much smaller than  $S_A$ . Taking a simple average, it is found that  $\langle S(1 \mu\text{m}) \rangle = 0.20 \langle S_A \rangle$ . The mean may be largely affected by extreme objects like 3C 368 (which itself may be contaminated by an M star—see below) and 3C 266

(which has a large red companion located orthogonally to the radio axis), so we have calculated the ratio of medians. It is lower, at 0.08.

We conclude that in essentially all objects, the infrared alignments that are seen in this sample are consistent with being produced by the long-wavelength tail of the aligned component (with a roughly flat spectral energy distribution) that dominates at shorter wavelengths.

We turn now to examine in detail those objects which show the strongest apparent alignments on Figure 6, with  $S(\lambda)$  at 1 μm comparable to  $S_A$  at 2500 Å on Figure 6. Principal among these are 3C 217, 3C 267, and the well-known case of 3C 368 observed by Chambers et al. (1988a) and Djorgovski et al. (1991). We review these cases in turn, along with 3C 356, which has been discussed both by Eales & Rawlings (1990) and by Eisenhardt & Chokshi (1990).

#### 4.1.1. 3C 217

The galaxy 3C 217 is an extremely active object. It has the second bluest 2500 Å to 1 μm color and the highest equivalent width of [O II] λ3727 in our sample. Its overall color is as blue as that of an Irr galaxy. The 2500 Å and [O II] λ3727 images are similar and show an elongated “football-shaped” structure symmetric about the peak and aligned at approximately 25° from the radio axis of this asymmetric and rather distorted double. Given the very blue color, a substantial contamination from the ultraviolet component would have been expected in the infrared. In fact, examination of the infrared image shows that the high moment in the infrared (equal to the moment at 2500 Å) is actually caused by a secondary peak located at the same position angle but slightly beyond the extent of the ultraviolet images (this component is seen in the 4100 Å image, so is definitely real). Within the area of the ultraviolet “football,” the infrared image is actually quite symmetric.

It is tempting to identify this secondary red peak as a companion object, particularly since the alignment with the radio axis is not particularly good. The peak is about the same distance from the nucleus as the radio hot spot, but at about 30° relative position angle (a displacement of 2''.4) from it. As mentioned above and discussed in more detail below, we find many similar red companion candidates in other objects with a wide range of position angles.

In short, we believe that the multicolor morphology of 3C 217 is consistent with the two-component old galaxy interpretation, despite the apparent similarity of the moment parameters as determined in the optical and in the infrared.

#### 4.1.2. 3C 267

The object 3C 267 is the most problematic in our sample. Unfortunately, it is the faintest object in the infrared and one of the faintest in the optical. Our data in all wave bands are thus of lower quality than for the other objects in the sample. Its own faintness in the infrared and the lack of any brighter objects nearby precluded our usual checks of the coregistration process. As a consequence, of all our images, this is the one in which we have least confidence, and we plan to take new observations of this object.

The optical image shows an elongated structure extending at P.A. = 130°, which is also seen in our composite infrared image. This structure is aligned at 30° to the radio source axis. Nevertheless, it is clear that the central area is redder than the southern extension by about 1 mag, although the  $(V-H)_{AB}$  color of this southern component (about 1.9 mag) is signifi-

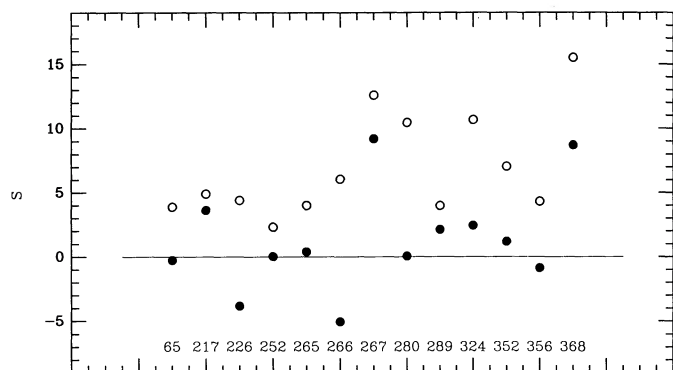


FIG. 6.—Moment parameter (along the preferred axis defined by the 2500 Å image),  $S(\lambda)$ , measured at 2500 Å (open symbols) and 1 μm (filled symbols) for all the objects in the sample. In every case  $S$  is substantially smaller in the infrared, indicating that a red symmetric component dominates at long wavelengths.

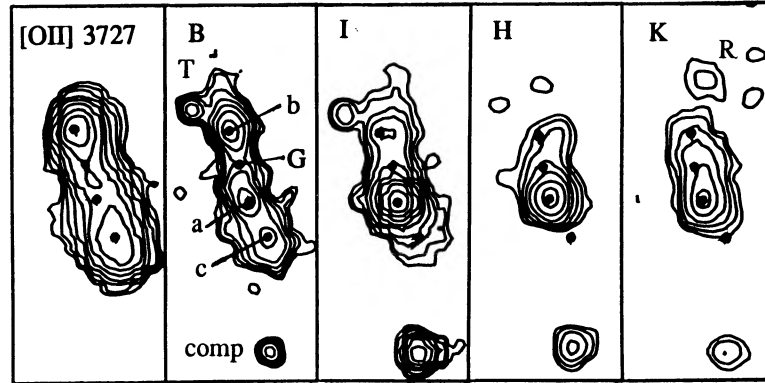


FIG. 7.—Detailed montage of 3C 368 identifying the various components discussed in the text. The brightest component (“a”) is very likely to be a superposed Galactic M star.

cantly redder than the aligned components in the other radio galaxies. It should be noted that this infrared “alignment” is at a relatively large angle to the radio source axis. We suspect that this red “aligned” component is either (a) similar to that seen in the other radio galaxies, except intrinsically redder, or (b) due to the presence of red “companions” interacting with the main galaxy, which our relatively poor-quality data has failed to resolve.

#### 4.1.3. 3C 368

The object 3C 368 was the first high-redshift radio galaxy to be imaged in the infrared (Chambers et al. 1988a), and the “infrared alignment” seen in this object stimulated much of the theoretical work discussed in § 1, on the expectation that this was a typical object. In fact, 3C 368 is extreme in its color (it is the bluest in the sample) and  $[O II] \lambda 3727$  line strength. It also provides the most striking example of the alignment effect at optical wavelengths, and some degree of alignment in the infrared is consequently not unexpected. An improved infrared image has been published by Djorgovski et al. (1991). A polar-

ization map at optical wavelengths has recently been published by Scarrott et al. (1990).

It is by now clear that 3C 368 is actually a considerably more complex system than the other radio galaxies in the sample. Two of us (Hammer et al. 1991) have recently suggested that the brightest component is a foreground object and have tentatively identified this as a Galactic M star on the basis of optical spectroscopy at high spatial resolution. Analysis of the present multicolor data supports this idea in the following way.

In describing the components of 3C 368 (see Fig. 7), we follow as much as possible the nomenclature of Hammer et al. (1991), making reference also to that of Djorgovski et al. (1991). The small-aperture colors of various components of the 3C 368 system were measured from the co-smoothed images. Aperture colors in a  $1''$  aperture were measured for the bright central component, “a,” for two locations at the local peaks in the rest-frame  $2500 \text{ \AA}$  and  $[O II] \lambda 3727$  images found to the north and south (“b” and “c”), and for a point midway between “a” and “b” which we have called “G.” Our “G” position is thus slightly to the north of the central peak in  $[O II] \lambda 3727$  (i.e., component “e” of Hammer et al. 1991), which is probably identified with the radio core component. We have also measured the colors through  $2''$  apertures of other objects in the field, including the faint star “comp” (again following Hammer et al. 1991), which is  $6''$  arcsec south of “a,” and the objects “T” and “R” (the latter following Djorgovski et al. 1991), which lie  $2''$  northeast and  $3''$  north, respectively, of “b.” Our “a” component is Djorgovski et al.’s (1991) “Q”; our “b” is their “A”; and our “G” must be close to their “K.”

These colors have been plotted on a two-color  $(B-I)_{AB}/(I-K)_{AB}$  diagram (Fig. 8), converting the “long continuum” image to the  $I$  band and applying reddening corrections to all objects. Because of the very long baseline in wavelength, this diagram is a powerful discriminant between Galactic stars and composite stellar systems, especially when the latter lie at high redshifts (see, e.g., Cowie et al. 1990). The figure shows a locus of Galactic stars, of power-law continua, and of Irr, Sbc, and E galaxies at redshifts  $0.0 < z < 2.0$ . Most of the objects in the field are Galactic stars, and they lie close to the expected track in this diagram. From its location on the diagram, the unrelated southern object “comp” is almost certainly a K7–M1 Galactic star, as was suggested from spectroscopic data by Hammer et al. (1991).

Of the components of the 3C 368 system itself, the northern

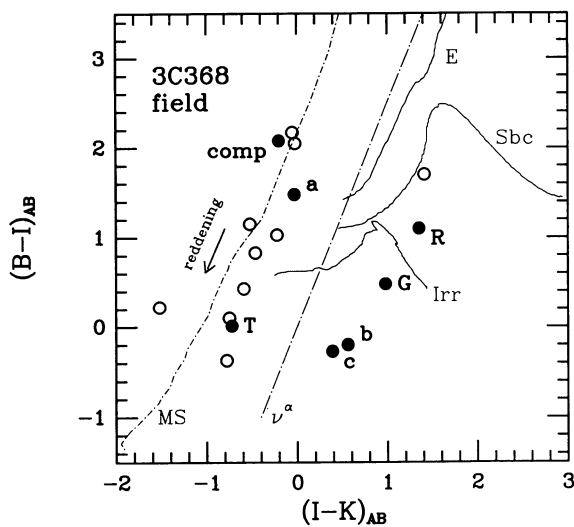


FIG. 8.— $(B-I)_{AB}/(I-K)_{AB}$  two-color diagram for objects in the 3C 368 field. The lines represent the stellar main sequence, power-law spectral energy distributions, and the colors of E, Sbc, and Irr galaxies as a function of  $z$  in the interval  $0 < z < 2$ . All the data points have been dereddened with the reddening vector shown.

and southern components (“b” and “c”) and the central location (“G”) have the colors of blue stellar systems at high redshifts ( $z > 1$ ). Components “b” and “c” have a flat spectral energy distribution between  $B$  and  $I$  and a gentle rise up to  $K$ . This is the signature of an extremely young starburst population (see, e.g., Bruzual 1983). The central component “G” is redder, more like an Irr galaxy at this redshift. The northernmost component “R” is also likely to be a stellar system at  $z = 1.1$ . It is significantly redder than the main components “b,” “c,” and “G,” and appears to have the colors of an Sbc galaxy. In marked contrast to these components, the bright central component “a” (and also the fainter northeastern object “T”) lie squarely on the “stellar” locus of Galactic stars. In particular, “a” lies close to the colors of the M star “comp.” Some admixture from an underlying high-redshift component, presumably with colors similar to those of “G,” has probably pulled the position of this component down a little on the figure. It should be noted that “a” does not have a power-law spectral energy distribution. Djorgovski et al. (1991) associated this component (their “Q”) with the radio core and identified it as an obscured quasar nucleus.

We take this analysis to provide important support for the identification of the brightest component “a” in the 3C 368 system as a foreground Galactic star. This will make the underlying galaxy somewhat bluer in  $(B-K)$ . Note, however, that even in this extremely blue object, the central regions (i.e., “G”) appear to be redder than the outermost parts “b” and “c,” as expected from the old galaxy hypothesis and as found in the outer objects in the sample.

We have estimated the contribution of the central star to the overall spectral energy distribution of 3C 368 as follows. The ratio of the peak surface brightnesses of component “a” and star “comp” is 3.0 in  $H$  and 3.3 in  $K$ , with the difference probably reflecting the greater contribution of the underlying galaxy in  $K$  (see Fig. 7). We can thus take 3.0 times the flux of the star in  $H$  and  $K$  [thus assuming that the contaminating star has the same  $(H-K)$  color as the star “comp”—a reasonable assumption within the accuracy of this exercise, since  $(H-K)$  changes little with spectral type] as upper limits to the contribution of the interloping star in 3C 368. The star has  $K_{AB} = 21.1$  in a 4" aperture. This causes the  $K$ -magnitude of the real 3C 368 to become 0.75 mag fainter. If we, less justifiably assume that the spectral energy distributions of the two stars are the same down to  $B$ , then we can estimate the contamination over the whole wavelength range. We find a contamination of 50% at  $K$ , 75% at  $I$ , and 17% in  $B$ . The  $(B-K)_{AB}$  color of the galaxy changes from 1.4 to 0.84. Henceforth we will use both the raw and “decontaminated” colors in the discussion to follow.

Clearly the infrared image of 3C 368 is aligned with the radio and optical axes even if the foreground star is removed. However, within the context of the old galaxy hypothesis, this object is so blue (regardless of whether the original or corrected colors are used) that the young component may completely swamp the underlying old component and an arbitrarily large amount of infrared alignment is “acceptable.” We noted above, however, that the central regions “G” do appear to be redder than the outer parts “b” and “c,” even in this extreme object.

#### 4.1.4. 3C 356

The situation with 3C 356 is confusing. Two comparably bright objects lie on the radio axis. The object is thus unique

within our sample. There is disagreement in the literature as to the location of the active nucleus: Eisenhardt & Chokshi (1990) considered the northern object to be the radio galaxy host and quoted the position of a central radio core (R. A. Laing 1990, private communication) to support this identification. In contrast, Eales & Rawlings (1990) also quoted a private communication from Laing of a core component collocated with the southern object. We have taken the northern object to be the radio galaxy on account of its higher ionization spectrum.

Our infrared image is similar to that of Eisenhardt & Chokshi (1990). The northern object is compact and almost unresolved. The southern object is more extended and diffuse. While aligned along the radio axis with respect to the northern object, it is itself slightly elongated along a roughly perpendicular direction in the infrared (see Fig. 2).

Our view on 3C 356 is that while both components unarguably lie on the radio axis, neither shows evidence in the infrared for elongation along that axis. Individually, therefore, neither shows evidence for infrared light that *must* come from a dynamically young component, and hence both could be composed of old stars. Our guess is that the southern component may be a companion galaxy that has wandered into the jet path.

With the possible exception of 3C 267, we conclude that all of the radio galaxies in the sample have individual morphologies at infrared wavelengths that are fully consistent with the idea that the light is dominated by a symmetric component, which plausibly has a spectral energy distribution similar to that of a gE galaxy, with only modest contamination from the long-wavelength tail of a much bluer, roughly “flat-spectrum,” component that is aligned with the radio axis.

It should be stressed that this analysis does not prove that the symmetric component is an extended mature galaxy. For instance, a compact quasar nucleus would have produced the same morphological result. However, given the original argument based on the small dispersion in the  $K-z$  relation, a gE host galaxy is the most plausible identification for this component. We believe that this analysis does prove that, for this sample (i.e., 3C radio galaxies at  $0.8 < z < 1.3$ ), morphological arguments *against* the old galaxy hypothesis based on the alignment of the infrared images (Chambers et al. 1988a; Eisenhardt & Chokshi 1990) are incorrect.

#### 4.2. Sizes of the Galaxies

If the red/visual light is dominated by the starlight from the old elliptical-like host galaxy, then the characteristic scale length of this light may provide constraints on the dynamical evolution of massive galaxies and/or the cosmological geometry.

With the exception of our CFHT image of 3C 65 obtained with the large-format  $256 \times 256$  array, our data are not ideally suited to such an investigation because of (a) the large pixel size of the data (up to  $0''.6$ ); (b) the indifferent image quality (typically  $1''.0-1''.3$ ); (c) subtle ghosting effects introduced by the median flat-fielding process. The latter arises because the median filter does not completely eliminate the effects of objects (and in particular the radio galaxy itself) in the frames used to construct the background image. This effect is most serious in the IRTF data, where the spatial separation of the positions in the mosaic is small. A thorough treatment of these effects to yield accurate scale sizes for these images is beyond the scope of this paper.

In the present work, the sizes of the radio galaxy images were analyzed only to the extent of satisfying ourselves that they were consistent with the old galaxy hypothesis. The radius  $r_{0.25}$  at which the Petrosian function  $\eta(r)$  (defined as the surface brightness at some radius divided by the average surface brightness within that radius) falls to 0.25 was determined (cf. Djorgovski & Spinrad 1981). A value of  $\eta = 0.25$  corresponds to a value of the Gunn-Oke structure parameter  $a$  (Gunn & Oke 1975) of  $\alpha = 0.50$ . This is a convenient value to choose, since Lilly & Prestage (1987) measured  $\alpha$  at 19.2 kpc radius for a sample of 23 radio galaxies with  $z < 0.1$  and found  $\langle \alpha \rangle = 0.5$ . We would therefore expect the radio galaxies to have  $\langle r_{0.25} \rangle$  in the range  $2'' < r_{0.25} < 3''$  for  $0.05 < q_0 < 0.5$ . The radio galaxies observed with UKIRT and CFHT span an (uncorrected) range  $1.7 < r_{0.25} < 3.3$ . Correction for seeing effects reduces the sizes of the smaller galaxies to around 1.3. The extended light associated with the blue aligned components would also tend to increase the effective sizes of the galaxies.

These sizes are thus consistent with the known sizes of the giant elliptical galaxies associated with powerful radio sources at low redshifts, to within the limitations of our data. This topic will be explored in more detail elsewhere.

### 5. RED COMPANION GALAXIES

One of the most striking features of our infrared data is the large number of relatively red companion objects that are found close to a large fraction of the radio galaxies. These companions are generally more prominent on our infrared images than at shorter wavelengths, at least in part because the strong alignment of the radio galaxy continuum is weaker or absent in the infrared. In some cases, these companions are responsible for the high ellipticities measured in the infrared, especially when the derived position angles are grossly misaligned with the radio source axes. Particularly good examples are provided by 3C 217, 3C 265, 3C 266, 3C 280, and 3C 368 (over a third of the sample observed here). We have identified these objects on Figure 2 with the letter "C." It should be noted that we have excluded blue continuum regions, especially when located along the radio axis, since these are likely to be part of the "alignment effect" (see, e.g., the many blue knots in 3C 265 and the blue companion to 3C 65). Companions may also be present in several other objects, such as 3C 324 and 3C 352, but these are less compelling, with the neighbor in question being farther away (3C 352) or not particularly red (3C 324). The properties of the most likely companion objects are summarized in Table 5.

In many cases these companions are distinctly redder than the radio galaxy itself when viewed over the full 2500 Å to 1 μm range. As well as being prominent in the infrared, they are seen on the "long continuum" images (just above the 4000 Å break) and are thus undoubtedly "real" objects. They are usually noticeably fainter in the "short continuum" images (at roughly

3500 Å) and are frequently absent at 2500 Å and in the [O II] λ3727 emission line.

We have crudely estimated the relative magnitudes of the radio galaxies and companions in the infrared by simply comparing their peak surface brightnesses. It is found that the companions range from 1.0–2.5 mag fainter than the radio galaxies and are located 2"0–4"5 (of order 20–45 kpc) away and span a wide range of position angles relative to the radio axis, with two at 80° relative P.A. Any companions that are significantly fainter, or are either closer to or farther away from the radio galaxy, would probably have been missed. It is possible that asymmetries in the infrared images of some other objects (e.g., 3C 226) may be caused by closer companions that we have been unable to resolve. It is also possible that the relatively large southern object in the 3C 356 system could be viewed as a "companion," although, as discussed above, it does lie on the radio axis.

Down to  $K = 19$ , there are 40,000 objects per square degree (Cowie et al. 1990), giving an average separation to random field objects of approximately 10". We have not considered objects more than 5" away to be "companions," so most of the claimed companions should be real. 3C 266 is behind Abell 1374 at  $z \approx 0.2$ , so a higher density of foreground objects might be expected in this case. However, objects at such low redshifts would be relatively blue.

Within our small sample, we find that the radio galaxies with the best examples of nearby red companions that are clearly *not* associated with the alignment effect (i.e., the five galaxies named above) are preferentially the bluest systems with the more striking optical alignment effects. A Mann-Whitney test indicates that this difference is significant at the 99.5% level.

Close interactions with companions have been proposed as the trigger for quasar, Seyfert, and starburst activity for some time (Toomre & Toomre 1972; Adams 1977; Stockton 1982; Hutchings et al. 1981), and there is a considerable body of evidence to support this idea (Sanders et al. 1988; Stockton 1990; Heckman 1990). Even gas-poor companions can disrupt the central galaxy and funnel gas into the central regions. It is therefore not too surprising that we find companions around these very powerful radio galaxies. Their significance in the context of this paper rest on two indirect arguments that they provide against Chambers & Charlot's (1990) scenario in which some of the  $z \approx 1$  radio galaxies are very young and are being formed by the radio activity itself.

First, it suggests that the radio activity is still being triggered in the  $z = 1$ , systems through mechanisms similar to those which operate in the present-day universe. If, as has been suggested (Chambers & Charlot 1990), some these radio sources are truly in dynamically young systems, and if young radio sources are indeed themselves responsible for the formation of much of the stellar populations in the host galaxies, then one might have expected to find quite different triggering mechanisms in operation. Second, the fact that these companions are usually redder than the radio galaxy suggests that some "old" galaxies, of lower but still comparable mass, have existed around the site of the radio galaxy for some time, presumably in the small group or cluster. This makes the presence of an old population in the main radio galaxy itself appear very natural.

### 6. GLOBAL CORRELATIONS WITH COLOR

The preceding quantitative examination of the morphologies of individual objects has provided important support for the hypothesis that these radio galaxies contain a luminous red

TABLE 5  
RED COMPANIONS

3C	$d$	P.A.	$ \Delta P.A. $	$\Delta K$
217.....	2"4	69°	29°	1.3
265.....	4.6	341	54	1.8
266.....	1.9	75	68	0.9
280.....	2.2	13	78	1.9
368.....	4.3	359	19	1.4

elliptical-like galaxy plus varying amounts of a blue extended and "aligned" active component. The infrared images are more compact than the optical images, showing weaker alignments with the radio axes. Those alignments that are seen in the infrared are explicable in terms of the infrared tail of a roughly flat-spectrum component that dominates in the ultraviolet.

In this section, we examine the global correlations with the overall 2500 Å to 1 μm color that would be expected in this picture in various parameters, the point being that the color should reflect the level of activity in each object. Curiously, we find that these correlations are not as compelling as we would have expected from the individual morphologies, although the statistical significance within this small sample is low.

We have constructed the 2500 Å to 1 μm color from our spectral energy distributions by interpolating or by using an extrapolation based on the empirical colors. As a true color, this parameter is uncertain at the 0.2 mag level, but it enables us to compare galaxies at different redshifts as consistently as possible.

### 6.1. The Color-Magnitude Relation

A correlation between color and luminosity would be expected, since the bluer objects should have a greater contribution, at all wavelengths, from the active aligned component. Such a correlation is indeed seen in the optical wave band as shown in Figure 9a, where we have plotted the absolute magnitude at 2500 Å against the overall 2500 Å to 1 μm color.

Although diluted by the uniform red component dominating at infrared wavelengths, a residual of this correlation should be apparent in the infrared, unless the active component has an extremely blue color. If the aligned active component had a uniformly flat spectral energy distribution in all objects, then an increase in luminosity at 1 μm of about 0.5 mag would be expected over the full 3 mag range of color present in the sample. This is shown in Figure 9b. A redder active component would produce a larger effect in the infrared. To eliminate this expected correlation between color and magnitude entirely

would of course require an infinitely blue active component, a possibility that can be ruled out because some residual alignment is seen in the infrared, indicating that some fraction of the infrared light is indeed produced from the aligned component.

We have plotted the 1 μm luminosity against the 2500 Å to 1 μm color in Figure 9b. A straightforward linear least-squares fit to these data produces an inverse correlation. This is driven by 3C 217, which is one of the bluest but faintest galaxies in the sample, and by 3C 65, which is the reddest and brightest! The remaining galaxies do show a trend in the desired sense, although it should be remembered that 3C 368, the second bluest object, may well be about 0.75 mag fainter if it is contaminated by a foreground object (see above).

Four possibilities present themselves. First, the observations could be in error for 3C 65 and 3C 217. This is very unlikely. The infrared photometry agrees well with the Lilly & Longair (1984) measurements, and in the case of 3C 217 there is good agreement in the present study between independent IRTF and UKIRT measurements. There are also independent reasons to think 3C 65 to be red and 3C 217 to be blue, in that these objects have the smallest and greatest equivalent widths for [O II] λ3727 in the sample.

Second, 3C 65 and 3C 217 may be statistical flukes within a small sample. This is still quite reasonable. A Pearson rank test gives only a very low correlation coefficient ( $r_s = 0.07$ ), indicating that there is an 80% chance that the observed distribution comes from an *uncorrelated* distribution. While a weak correlation in the opposite sense would have been expected, the chance of observing the observed distribution is still presumably reasonably high. This possible explanation can of course be tested with a larger sample. Until such a larger sample is studied, this explanation for the form of Figure 9b is our preferred one.

Third, 3C 65 and 3C 217 may represent different physical situations where the standard old galaxy picture would not apply. The object 3C 65 could have a red nonstellar nucleus, for example (but recall that its emission lines are relatively weak), while 3C 217 could represent a new class of sub-

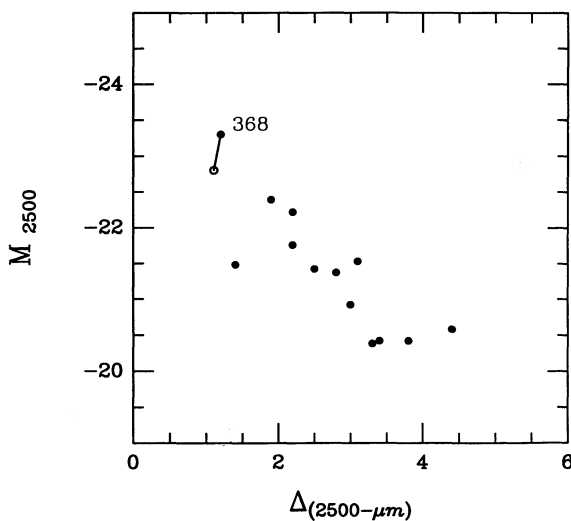


FIG. 9a

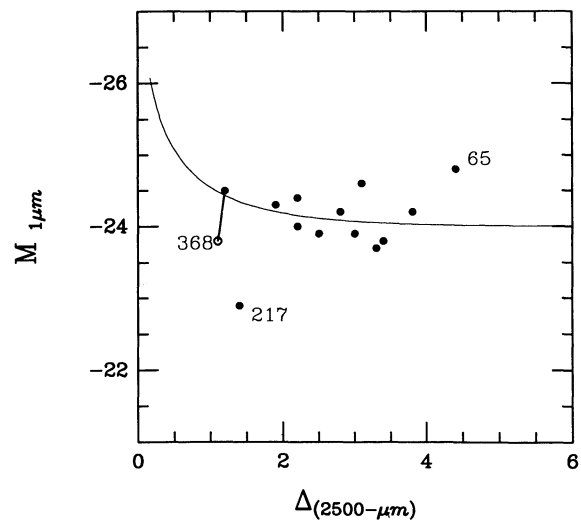


FIG. 9b

FIG. 9.—Color—absolute magnitude diagrams for the galaxies in the sample: (a) 2500 Å to 1 μm color vs. 2500 Å absolute magnitude and (b) the same color vs. 1 μm absolute magnitude. The curve in (b) represents the expected effect of adding a flat-spectrum component to a gE galaxy. 3C 368 has been shown as observed (solid symbol) and after attempted removal of the putative M star (filled symbol).

luminous radio galaxies. We are naturally unwilling to advocate such an unattractive interpretation at this stage.

Finally, the diagram could represent the true situation in which there is an inverse correlation between color and luminosity, in the sense that the reddest objects are brighter. Within the context of the old-galaxy interpretation, this would require that the strength of the active component was in some way related to the mass of the galaxy. It is possible to envisage a scenario in which more massive galaxies get rid of their gas at earlier times, so that the most vigorous jet-induced star formation at  $z = 1$  occurred in lower mass systems. In this sense the small dispersion in the  $K$ - $z$  relation would be at some level a coincidence; the true dispersion in the  $K$ -magnitudes of the underlying galaxies would actually be larger, with the fainter members being boosted by the additional active component. This option is similarly unattractive.

We note in passing that alternative models in which there is a wide range of ages (e.g., the Chambers & Charlot 1990 model) also predict a correlation between color and luminosity in the sense that the brighter objects should be bluer.

### 6.2. Elongation as a Function of Color

In the simple model where a blue aligned component is added to a red symmetric galaxy, it would be expected that the alignment effects would be most apparent in the bluest objects, since these will have the largest contribution from the blue aligned component. Of course, some blue objects may be symmetrical if the active component is itself not elongated, and a variation in spectral index of the aligned component may further dilute any correlation, but red objects would not be expected to show strong alignments. Such an overall trend was demonstrated by Lilly (1989), who showed that the optically most aligned objects in the original McCarthy et al. (1987b) sample had the bluest colors in  $(r - K)$ . Furthermore, the very red "1 jansky" identifications presented by Lilly (1989) showed virtually no alignment effect even at very short wavelengths.

In Figure 10a we have plotted the  $S_A$  parameter, defined at roughly 2500 Å, against the overall rest-frame (2500 Å to 1 μm)

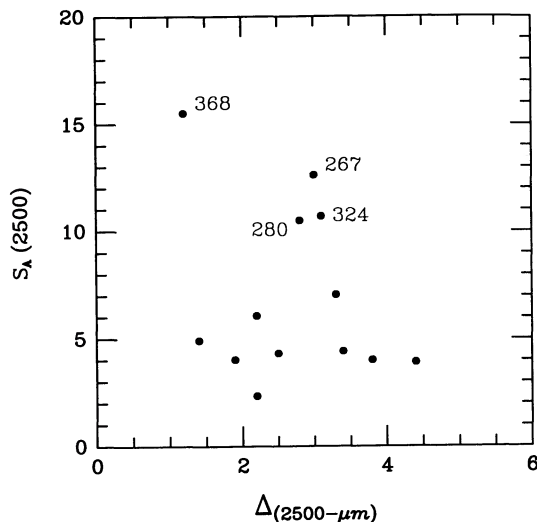


FIG. 10a

color for the sample of objects studied here. The most aligned objects, 3C 368, 3C 267, 3C 280, and 3C 324, all have colors 1.5 mag bluer than the reddest, and much more symmetrical, radio galaxy 3C 65.

To look directly at this effect in the infrared, we have plotted in Figure 10b the value of  $S(1 \mu\text{m})$  measured in the infrared (with the preferred axis again being defined by the short-wavelength images) against the overall color. A more confusing diagram results, partly because of the relatively large elongation of the "misaligned" 3C 266 (recall that this was due to a red companion lying perpendicular to the radio axis) and the anomalously high elongation of 3C 267. The remaining objects have a distribution similar to that in Figure 10a, in that there are no very red, very aligned objects, although it is again striking in this figure how much smaller the infrared moments are relative to the optical ones.

### 7. THE ALIGNED COMPONENT

The actual nature of the active, aligned component has not been important for most of the foregoing discussion in this paper, which has been concerned primarily with establishing the presence of a central symmetric red component in these galaxies. We are presently analyzing our images with a view to trying to understand the nature of the active component, and our conclusions will be presented elsewhere. Nevertheless, in this section we present a few general comments concerning the alignment effect that have struck us in our initial examination of the images, bearing in mind that this is the first complete and statistically well-defined sample to be subjected to systematic scrutiny.

First, the "alignment effect" is by no means perfect. Many striking elongated objects have position angles that are displaced from the radio axis by several tens of degrees. The spread in relative position angles displayed in the upper two panels of Figure 4 is certainly not measurement error, as cursory examination of 3C 352 reveals.

Second, we note that the distributions of 2500 Å continuum and  $[\text{O II}] \lambda 3727$  emission-line gas are often strikingly similar.

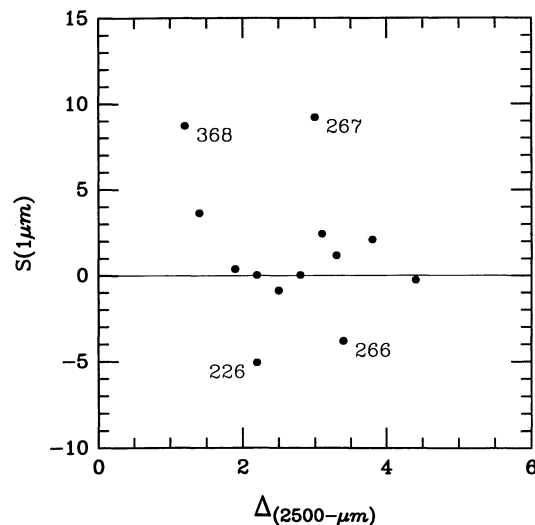


FIG. 10b

FIG. 10.—Relationship between the overall 2500 Å to 1 μm color and the degree of alignment, parameterized by the moment  $S$  along the axis defined by the 2500 Å image, determined (a) at 2500 Å and (b) at 1 μm.

Indeed, we initially used the [O II]  $\lambda 3727$  image to define the “active” component, before deciding that the 2500 Å continuum image was a more logical choice. The results changed very little when this change was made, as is seen by comparing the values of  $S$  for the 2500 Å continuum and [O II]  $\lambda 3727$  images listed in Table 3.

Finally, we note that the “quality” of the alignment (meaning the degree of elongation *and* the relative position angle) depends strongly on the size of the radio source. The objects 266, 3C 324, and 3C 368 are all small double sources with separations of 10" or smaller (roughly 90 kpc at  $z \approx 1$ ). This trend is shown in Figure 11, where we have plotted the short-wavelength  $S_A$  parameter against the projected radio separation. We have plotted both  $S_A$  and  $S_A \times \cos 2\theta$ , where  $\theta$  is the misalignment angle between the optical and radio axes. McCarthy et al. (1990) have already noted that the elongated components are frequently one-sided and in these cases appear always to lie toward the nearer radio lobe.

### 8. OBJECTS AT HIGHER REDSHIFTS

Viewed as a whole, we believe that the results of this investigation support the “old galaxy” interpretation of these objects. The individual morphologies of objects are certainly generally consistent with this model, since all objects (with the possible exception of 3C 267) show the signature of a centrally concentrated symmetric red component that dominates the light to the degree required to explain the small scatter in the  $K$ - $z$  diagram. While the global correlations with color are not seen as strongly as expected, the sample used here is small.

A key question for the future is whether the quantitative analysis of infrared morphologies will continue to support this conclusion at higher redshifts, where the cosmogonic issues become more acute. The  $K$ - $z$  relation shows smaller scatter out to at least  $z = 3.5$  (see, e.g., Lilly 1991). We have begun a program to carry out similar multicolor observations on samples of objects at these higher redshifts.

In the meantime, two comments are warranted: First, at higher redshifts, the infrared passbands are redshifted to shorter wavelengths, and asymmetries are expected to become

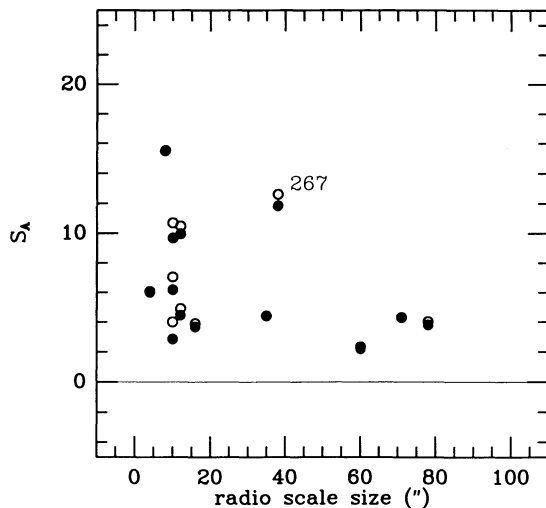


FIG. 11.—Diagram showing the tendency for the most dramatic alignment effects to occur in objects associated with physically small radio sources. Open symbols represent  $S_A$ ; filled symbols are  $S_A \times \cos 2\theta$ , where  $\theta$  is the misalignment angle between the radio source axis and the 2500 Å axis.

more apparent as the aligned component contributes a greater fraction of the flux density. Nevertheless, the small dispersion in infrared magnitude may be preserved until the average contamination approaches 40% depending on the variation within the sample), by which point the most extreme objects may have contaminations as high as 70%. Figure 1 stresses how dramatic alignments can be produced by components that contribute less than 50% of the total flux density. Second, it should be borne in mind that most of the galaxies that have had redshifts measured at  $z > 2$  have been selected on account of their “ultrasteep” radio spectra (e.g., Chambers et al. 1988b; Chambers et al. 1990; McCarthy et al. 1991). There appears to be a correlation between the steepness of the radio spectral index and the strength of the active component (Lilly 1989), and hence one might expect that these objects are unusually active, and therefore more aligned than more typical radio galaxies.

We suspect that the levels of contamination found in the present study could be increased significantly, thereby producing more dramatic morphological effects, without substantially increasing the scatter in the  $K$ - $z$  relation.

### 9. SUMMARY

Qualitative and quantitative analysis of a homogeneous set of multicolor line and continuum images of a complete sample of 3C radio galaxies at  $0.8 < z < 1.3$  has led us to the following conclusions:

1. The infrared morphologies are much more symmetric than those at optical wavelengths. Although several of the infrared images are aligned with the radio axes, quantitative measures of the asymmetry show a progressive *reduction* as one goes from rest-frame 2500 Å to  $1 \mu\text{m}$ , as is to be expected if a symmetric component increasingly dominates at the longer wavelengths. This is consistent with the “old galaxy hypothesis” for these galaxies, whereby the small scatter in the  $K$ - $z$  relation is produced by a homogeneous population of mature host galaxies.

2. A spectral decomposition based on these quantitative morphological parameters strongly suggests that the “active” component, which dominates in the ultraviolet wave band and is usually roughly aligned with the radio source axis, has a roughly flat spectral energy distribution in  $f_\nu$  between 2500 Å and  $1 \mu\text{m}$ . Similarly, the data are consistent with the “symmetric” component having a red spectral energy distribution similar to that of a gE galaxy, although the spectral decomposition is not unique.

3. Typical 3C radio galaxies at  $z = 1$  probably have about 10% of their rest-frame  $1 \mu\text{m}$  light produced by the active component. The more active objects have larger contributions. Nevertheless, these modest contaminating components are insufficient to perturb either the scatter or the continuity of the observed  $K$ - $z$  relation.

4. The angular sizes of the infrared images of the radio galaxies are consistent with the known sizes of the giant elliptical galaxies associated with powerful radio sources at low redshifts for reasonable cosmologies, i.e.,  $0.05 < q_0 < 0.5$ .

5. A significant fraction (5/13) of these radio galaxies are accompanied by nearby red companion galaxies that are prominent on the infrared images. These are 1–2 mag fainter than the main galaxy, but are usually redder in overall color and usually have little or no associated [O II] emission. The presence of these red companions suggests that “conventional” triggers for the radio sources are still oper-

ating at  $z > 1$ , and that, regardless of the evolutionary state of the radio galaxy, at least some old galaxies exist around the central object.

6. Photometric analysis of the components of the complex object 3C 368 supports the view that the brightest component is a foreground Galactic M star.

7. While there is a strong correlation between the overall color and absolute magnitude at short wavelengths, there is little evidence for the expected correlation between color and absolute magnitude in the infrared, although our sample is small and, given the intrinsic scatter expected, the statistics are poor.

8. As expected, the most aligned objects are the ones with the bluest overall colors, since these have the strongest active components. These objects also have the smallest projected radio separations.

Viewed as a whole, we take the results of this study to be completely consistent with the view that these radio galaxies form a homogeneous population of mature gE-type galaxies undergoing, to various degrees, bursts of star formation associated with the radio source activity, as originally proposed by Lilly & Longair (1984) and further refined by Lilly (1989) to explain the small scatter in the  $K$ - $z$  relation and the large range of optical-infrared colors.

*Note added in manuscript.*—On 1991 May 30 one of us (M. A. R) obtained an improved infrared image of 3C 267 using the

NICMOS3 ( $256 \times 256$ ) device at CFHT. The high resolution and large field of view of this image enabled an extremely accurate coregistration with the optical data. The infrared emission is elongated, at an angle of 30 degrees from the radio axis, but it is not colocated with the aligned optical emission: the peak of the infrared emission lies at its southwest end, and coincides with the northeast end of the aligned optical emission. The new data also confirm that this galaxy has a fairly blue optical to infrared color.

The galaxy 3C 267 is now easily interpreted as an evolved host galaxy with a red extension to the north, possibly due to unresolved companions, and a flat-spectrum component extending toward the southwest along the radio axis.

We are very appreciative of the outstanding technical assistance of telescope operators and day crews at the UKIRT, CFHT, IRTF, and UH 2.2 m telescopes on Mauna Kea. We thank the referee for his or her very careful reading of the original manuscript and perceptive comments. We also acknowledge useful discussions with Ruth Daly, Ken Chambers, Pat McCarthy, Peter Eisenhardt, James Dunlop, Richard Elston, David de Young, and Buell Jannuzi. This work was supported by the NSF through grants AST 87-18275 and AST 87-15330, by the State of Hawaii, and, in its final stages, by the NSERC of Canada.

#### REFERENCES

- Adams, T. A. 1977, *ApJS*, 33, 19  
 Alexander, P., & Leahy, P. J. 1987, *MNRAS*, 225, 1P  
 Barthel, P. D. 1989, *ApJ*, 336, 606  
 Bithell, M., & Rees, M. J. 1990, *MNRAS*, 242, 570  
 Bruzual A., G. 1983, *ApJ*, 273, 105  
 Burstein, D., & Heiles, C. 1982, *AJ*, 87, 1165  
 Chambers, K. C., & Charlot, S. 1990, *ApJ*, 348, L1  
 Chambers, K. C., & McCarthy, P. J. 1990, *ApJ*, 354, L9  
 Chambers, K. C., Miley, G., & Joyce, R. R. 1988a, *ApJ*, 329, L75  
 Chambers, K. C., Miley, G., & van Breugel, W. 1987, *Nature*, 329, 609  
 ———. 1990, *ApJ*, 363, 21  
 Chiosi, C., & Maeder, A. 1986, *ARA&A*, 24, 329  
 Coleman, G. D., Wu, C.-C., & Weedman, D. W. 1980, *ApJS*, 43, 393  
 Cowie, L. L., Gardner, J. P., Lilly, S. J., & McLean, I. S. 1990, *ApJ*, 360, L1  
 Daly, R. A. 1990a, *ApJ*, 355, 416  
 ———. 1990b, preprint  
 ———. 1992, *ApJ*, in press  
 de Young, D. S. 1989, *ApJ*, 342, L59  
 di Serego Alighieri, S., Fosbury, R. A. E., Quinn, P. J., & Tadhunter, C. N. 1989, *Nature*, 341, 307  
 Djorgovski, S., & Spinrad, H. 1981, *ApJ*, 251, 417  
 Djorgovski, S., Weir, N., Matthews, K., & Graham, J. 1991, in *ASP Conf. Ser. 14*, with *Infrared Arrays*, ed. R. Elston (San Francisco: ASP), in press  
 Dunlop, J. S., Guiderdoni, B., Rocca-Volmerange, B., Peacock, J. A., & Longair, M. S. 1989, *MNRAS*, 240, 257  
 Eales, S. A., & Rawlings, S. 1990, *MNRAS*, 243, 1P  
 Eisenhardt, P., & Chokshi, A. 1990, *ApJ*, 351, L9  
 Eisenhardt, P., Chokshi, A., Dickenson, M., Spinrad, H., Djorgovski, S. G., & McCarthy, P. 1991, in *ASP Conf. Ser. 14*, *Astrophysics with Infrared Arrays*, ed. R. Elston (San Francisco: ASP), in press  
 Eisenhardt, P., & Lebofsky, M. J. 1987, *ApJ*, 316, 70  
 Elias, J. H., Frogel, J. A., Matthews, K., & Neugebauer, G. 1982, *AJ*, 87, 1029  
 Gunn, J. E., & Oke, J. B. 1975, *ApJ*, 195, 255  
 Hammer, F., & Le Fèvre, O. 1990, *ApJ*, 357, 38  
 Hammer, F., Le Fèvre, O., & Proust, D. 1991, *ApJ*, 374, 91  
 Heckman, T. M. 1990, in *IAU Colloq. 124*, *Paired and Interacting Galaxies*, ed. J. W. Sulentic (NASA CP-3098), in press  
 Hutchings, J. B., Crampton, D., Campbell, B., & Pritchett, C. 1981, *ApJ*, 274, 743  
 Jenkins, C. J., Pooley, G. G., & Riley, J. M. 1977, *MNRAS*, 84, 61  
 Laing, R. A., Riley, J. M., & Longair, M. S. 1983, *MNRAS*, 294, 151  
 Landolt, A. U. 1983, *AJ*, 88, 439  
 Leahy, P. J. 1990, private communication  
 Le Fèvre, O., & Hammer, F. 1988, *ApJ*, 333, L37  
 Le Fèvre, O., Hammer, F., & Jones, J. 1988, *ApJ*, 331, L73  
 Lilly, S. J. 1988, *ApJ*, 333, 161  
 ———. 1989, *ApJ*, 340, 77  
 ———. 1990, in *ASP Conf. Ser. 9*, *The Evolution of the Universe of Galaxies*, ed. R. G. Kron (Dordrecht: Kluwer), 344  
 ———. 1991, in *Observational Tests of Inflation*, ed. T. Shanks (Dordrecht: Kluwer), in press  
 Lilly, S. J., & Longair, M. S. 1984, *MNRAS*, 211, 833  
 Lilly, S. J., Longair, M. S., & Allington-Smith, J. R. 1985, *MNRAS*, 215, 37  
 Lilly, S. J., & McLean, I. S. 1989, *ApJ*, 346, L65  
 Lilly, S. J., & Prestage, R. M. 1987, *MNRAS*, 225, 531  
 McCarthy, P. J., Kapahi, V. K., van Breugel, W., & Subrahmanya, C. R. 1990, *AJ*, 100  
 McCarthy, P. J., Spinrad, H., Djorgovski, S., Strauss, M. A., van Breugel, W., & Liebert, J. 1987a, *ApJ*, 319, L39  
 McCarthy, P. J., van Breugel, W., Kapahi, V. K., & Subrahmanya, C. R. 1991, *ApJ*, 371, 478  
 McCarthy, P. J., van Breugel, W., Spinrad, H., & Djorgovski, S. 1987b, *ApJ*, 321, L29  
 Oke, J. B., & Gunn, J. E. 1983, *ApJ*, 266, 713  
 Pedely, J. A., Rudnick, L. A., McCarthy, P. J., & Spinrad, H. 1989, *AJ*, 97, 647  
 Rawlings, S., Eales, S. A., & Warren, S. 1990, *MNRAS*, 243, 14P  
 Rees, M. J. 1989, *MNRAS*, 242, 1P  
 Sanders, D. B., Soifer, B. T., Elias, J. H., Madore, B. F., Matthews, K., Neugebauer, G., & Scoville, N. Z. 1988, *ApJ*, 325, 74  
 Scarrott, S. M., Rolph, C. D., & Tadhunter, C. N. 1990, *MNRAS*, 243, 5P  
 Spinrad, H., Djorgovski, S., Marr, J., & Aguilar, L. 1985, *PASP*, 97, 932  
 Stockton, A. 1982, *ApJ*, 257, 33.  
 ———. 1990, in *Dynamics and Interactions of Galaxies*, ed. R. Wielen (Heidelberg: Springer-Verlag), 440  
 Stockton, A., & Lilly, S. J. 1988, in *IAU Symp. 134*, *Active Galactic Nuclei*, ed. D. E. Osterbrock & J. S. Miller (Dordrecht: Kluwer), 541  
 Toomre, A., & Toomre, J. 1972, *ApJ*, 178, 623  
 van Breugel, W. J. M., & McCarthy, P. K. 1990, in *ASP Conf. Ser. 9*, *The Evolution of the Universe of Galaxies* ed. R. G. Kron (Dordrecht: Kluwer), 359